NASA TN D-1658

TECHNICAL NOTE

D-1658

EROSION RESISTANCE AND FAILURE MECHANISMS OF SEVERAL NOZZLE MATERIALS IN A SMALL SOLID-PROPELLANT ROCKET ENGINE

By Robert A. Signorelli and James R. Johnston

Lewis Research Center
Cleveland, Ohio

NATIONAL AERONAUTICS AND SPACE ADMINISTRATION
WASHINGTON

February 1963

NATIONAL AERONAUTICS AND SPACE ADMINISTRATION

TECHNICAL NOTE D-1658

EROSION RESISTANCE AND FAILURE MECHANISMS OF SEVERAL NOZZLE MATERIALS IN A SMALL SOLID-PROPELLANT ROCKET ENGINE

By Robert A. Signorelli and James R. Johnston

SUMMARY

A small-scale end-burning solid-propellant rocket-engine facility was constructed, and an investigation was conducted to study uncooled rocket-nozzle insert materials under carefully controlled test conditions. Relative performance and metallurgical failure mechanisms were determined for 12 nozzle materials, including refractory metals, graphites, cermets, reinforced plastics, and a ceramic. A nonaluminized propellant, Arcite 368, which has a theoretical flame temperature of 4700° F was used. The engine was designed to operate at a chamber pressure of 1000 pounds per square inch for 30 seconds with a nozzle-throat diameter of 0.289 inch.

With the exception of molybdenum, all of the materials eroded to some degree. In general, the cermet and ceramic materials eroded very little (1 to 2 mils), tungsten and ZT graphite eroded moderately (5 to 9.5 mils), and the molded graphites and the 40-percent-resin phenolic-refrasil-composite material eroded extensively (up to 30.5 mils). The 20-percent-resin phenolic-refrasil and the phenolic-graphite materials eroded drastically (up to 54 mils), while complete failure occurred with phenolic-nylon material. The cermet and ceramic nozzles cracked extensively both radially and axially as a result of thermal stresses. Oxidation is believed to be the primary mechanism by which material was removed from the tungsten nozzle. Material removal from the graphite nozzles is attributed to oxidation coupled with mechanical erosion. Temperature measurements made with molybdenum and graphite nozzles indicated that the maximum throat-surface temperatures were slightly less than 3000° F, which is considerably below the 4700° F flame temperature.

A technique for propellant burning-surface modification was developed involving internal ballistic formulas, which permits the systematic variation of engine chamber pressure.

INTRODUCTION

Solid-propellant rockets have been used more extensively for large flight vehicles with the availability of high specific-impulse propellants. Not only has the size increased but also the firing duration and the flame temperature.

The development of these solid-propellant rockets presents several materials problems. The provision of satisfactory materials for nozzles is one of the more critical problems. This normally uncooled component must withstand high temperature, high velocity, erosive, corrosive exhaust gases that often contain abrasive particles of metallic oxides. The metallic-oxide particles result from the metal powders added to some propellants to increase specific impulse. The flame temperatures of some propellants currently in use are over 6000° F. Flame temperatures as high as 8000° F have been predicted within 10 years (ref. 1). In addition to the higher flame temperatures, these propellants probably will be more reactive, since oxidizers such as fluorine compounds may be employed (ref. 2). Thus, the problem of providing satisfactory materials for solid-propellant rocket nozzles will become even more difficult.

Material can be removed from the nozzle by thermal, chemical, or mechanical means, and the structural integrity of the nozzle can be destroyed by cracking as a result of thermal shock. Because of the complex combinations of failure mechanisms that may occur, prediction cannot be made of the behavior of potential nozzle materials based on physical-property data or simple laboratory tests. Ideally, rocket-nozzle-material-failure studies should be conducted with full-scale rocket engines; however, the vast quantities of propellant and the large test installations and components required to investigate materials thoroughly as full-size nozzles are obviously too costly. Screening tests made with oxyacetylene torches, plasmas, and small liquid-propellant rocket engines (refs. 3 to 6) have been used to study potential nozzle materials. These tests are relatively inexpensive and have generated useful data; however, the results are not always indicative of the relative behavior of materials in full-scale solid-propellant rockets. Torches and plasma guns provide hot gases but not the abrasive reactive gases of solid propellants. The addition of metallic oxides to liquid propellants also does not result in exhaust gases that duplicate those of solid propellants.

The conditions of full-scale rocket-engine firings can be simulated more nearly by use of small-scale solid-propellant engines. Most of the important parameters such as mass-flow rate per unit area of nozzle throat, exhaust-gas temperature, exhaust products, and gas velocity are readily duplicated. Two major conditions, the nozzle-surface temperature history and nozzle thermal stresses, may be influenced by size effects; however, the nozzle-surface temperature history of a large nozzle can be closely approximated in a small-scale nozzle by selection of the wall thickness so that the heat-sink effect is similar. Nozzle thermal stresses are influenced by many interrelated factors of size and shape as well as by the specific installation configuration. As a result, duplication of the range of thermal stresses that can occur in full-scale nozzles with a single small-scale rocket nozzle is impractical if not impossible. Despite this shortcoming, however, the advantage of small-scale solid-propellant rocket-engine tests over other methods of testing nozzle materials has generally been recognized, and many tests of various potential nozzle materials have been conducted over the years. Most tests were of the "go" or "no-go" type. The results of these tests are valuable for a specific rocket-development program, but variation of test conditions often found in these investigations detracted from the general applicability of comparisons of the relative performance of nozzle materials.

A program was therefore initiated at the Lewis Research Center to investigate nozzle materials in a small-scale rocket engine by using carefully controlled test conditions. By maintaining uniformity of test conditions, it was believed that more realistic comparisons of the relative performance of nozzle materials could be made, and that failure-mechanism studies of materials under the known conditions of this investigation would permit more meaningful predictions of nozzle-material performance under other conditions. Accordingly, relative performance of various nozzle materials was determined, and nozzle-failure mechanisms were studied. In the small-scale rocket used, special attention was given to the control of key variables such as nozzle geometry, initial chamber pressure, and the extent of exhaust-gas contamination by extraneous materials.

The program was planned to include studies with several solid propellants and various promising nozzle materials. These included refractory metals and compounds, ceramics, cermets, and composite materials. This report describes the development of facilities and operating procedures for firings with a commonly used nonaluminized propellant, Arcite 368, and presents the results obtained for a group of 12 materials investigated using this propellant. Performance of these materials was compared on the basis of erosion-resistance data obtained from chamber-pressure traces and postfiring analysis. The rocket engine was designed to operate at a chamber pressure of 1000 pounds per square inch for about 30 seconds with a nozzle-throat diameter of 0.289 inch.

NOZZLE INSERTS

Materials

The general classes of materials investigated were graphites, refractory metals, ceramics, cermets, and reinforced-phenolic-composite materials. The specific materials investigated are listed in table I. Molybdenum, tungsten, and the graphites were obtained in the form of billets or bar stock from which nozzles were machined. The arc-cast molybdenum and the graphites were obtained from commercial sources, while the tungsten was arc cast at the Lewis Research Center. The reinforced-plastic nozzles were obtained from commercial sources as finished nozzles. The ATJ, Speer 3499, and ZT graphite nozzles were machined so that the axial direction, or direction of gas flow, was parallel to the direction in which the graphites were pressed during molding. The reinforced-plastic nozzles were cross ply with the fiber cloth plies in a plane perpendicular to the axial direction of the nozzle insert.

Nozzle Configuration

The dimensions and contour of the nozzle inserts used in this investigation are shown in figure 1. The nozzle was a conventional converging-diverging type with entrance and exit angles of 120° and 30°, respectively. The expansion ratio

was approximately 8 to 1. The throat diameter of the nozzle insert was 0.289 ± 0.001 inch.

The small size of the insert was an advantage in readily obtaining nozzle materials, particularly experimental materials, and in minimizing the size and the cost of the test installation and the propellant grains. For example, use of a nozzle with a throat diameter of 1 inch would have resulted in a propellant-consumption rate greater than 11 times that used with the 0.289-inch nozzle. Also, by specifying these relatively small nozzles, operational hazards were reduced, whereas the throat dimensions were still large enough to permit normal machining techniques for the internal contours.

The choice of a nozzle insert having these relatively small dimensions introduces the possibility of size-factor effects. As indicated earlier, several engine conditions can readily be duplicated independently of size, whereas the nozzle-surface temperature history and thermal stresses may be influenced by nozzle size. It can be shown by use of the dimensionless heat-transfer-parameter data presented graphically in reference 7 that the surface temperature history in a large nozzle can be closely approximated in a small nozzle by selection of a suitable wall thickness. In general, typical large nozzles (7- to 8-in. throat diam.) have wall thicknesses of the order of 10 to 20 percent of the throat diameter. The corresponding wall thicknesses in a subscale nozzle (0.3- to 0.5-in. throat diam.) would be of the order of 100 to 150 percent of the throat diameter to obtain a similar heat-sink effect and, accordingly, to effect a comparable temperature history. The effect of nozzle size on thermal stresses, however, is quite complex and cannot be determined readily. This effect and its implications with respect to the results of this investigation are discussed in the DISCUSSION OF RESULTS section. It will be shown by stress calculations that the thermal stresses encountered in the small nozzle of this investigation are lower than those in a typical full-scale nozzle.

TEST FACILITIES

Rocket Engine

The general configuration of the rocket test engine is shown in figure 2. The engine consisted essentially of an uncooled heavy walled steel tube open at each end with provision for mounting the nozzle insert in a removable retainer. The propellant grain was inserted from the head end of the engine and was held in place by a steel end closure. Neoprene O rings were used to seal against gas leakage. The nozzle retainer and the steel end closure were held in place with segmented steel retaining rings. The retaining ring at the nozzle end was designed to fail in shear to provide overpressure protection.

Insulation was not applied to the internal surfaces of the engine tube or to the internal end face of the nozzle retainer to prevent contamination of exhaust gases. The cardboard tube around the propellant was essentially unaffected during firing and thus did not contaminate the gases. The heavy steel wall construction of the engine obviated the need for insulation.

Nozzle Installation

The nozzle retainer and insert assembly is shown in figure 1. The outside cylindrical surfaces of the nozzle inserts were coated by flame spraying with zirconium oxide to a thickness of 0.05 inch. An epoxy asbestos resin mixture was then cast between the coated nozzle and a steel sleeve.

The zirconium oxide - epoxy asbestos insulation was used to reduce the heat loss from the nozzle insert to the steel retainer. The sleeve and nozzle assembly was inserted into the heavy steel nozzle retainer. A conventional neoprene O ring seal was used to seal against gas leakage. The removable steel sleeve was used to facilitate disassembly after firing without damaging the nozzle insert.

Propellant

The propellant grains used in this investigation were procured from the Atlantic Research Corporation. The propellant designation was Arcite 368, a non-aluminized polyvinylchloride ammonium perchlorate formulation. An as-received propellant grain is shown installed in the engine in figure 2. The end-burning grains were formed by sealing precast cylinders of propellant into cardboard tubes with a polyurethane inhibiting compound. An aluminum head plate was also bonded to one end face of the propellant to facilitate retention of the grain within the rocket engine. The length and diameter of the propellant were chosen to provide approximately 30 seconds of burning time at a chamber pressure of 1000 pounds per square inch.

Instrumentation

Conventional pressure transducers were used to measure chamber pressure. Pressure data were recorded on a multichannel oscillograph and on a strip-chart potentiometer. The location of the pressure taps is shown in figure 2. Nozzle inserts of several materials were instrumented at four positions (fig. 3). In each firing, Chromel-Alumel thermocouples were used at three stations, and a molybdenum-tungsten thermocouple was used at the fourth station. Since the Chromel-Alumel thermocouples were only suitable for temperatures up to 2500° F, the molybdenum-tungsten thermocouple was added to extend the measurement capability to 4000° F. During each run, all temperature data were recorded simultaneously on an oscillograph.

TEST PROCEDURES

Pretest Preparation

Prior to each firing, the chamber-pressure sensing and recording instrumentation was calibrated. Both pressure transducers were calibrated against a laboratory test gage having a precision of ±2 pounds per square inch.

Since the burning rate of the propellant was temperature sensitive, propel-

lant grains were maintained at 70° ± 2° F in a temperature-controlled storage chest. Each propellant grain was removed from storage shortly before installation and firing. The rocket-engine test stand was located within a heated building; thus, a relatively stable ambient temperature environment was provided for the tests. The propellant was ignited with a squib and pellet igniter electrically energized by wires inserted through the nozzle.

Propellant Burning Surface Modifications

Theoretically, the chamber pressure of an end-burning rocket would be constant throughout the firing if no nozzle erosion occurred. A stable chamber pressure, however, is often not obtained in practice because of variations in propellant-burning characteristics. Such a chamber-pressure variation (fig. 4(a)) was obtained in this investigation from preliminary firings with as-received propellant grains. The pressure increased gradually over a period of 8 to 10 seconds before stabilizing at design pressure. Since the success of the entire series of tests depended on a comparison of the results from one test with those of another, it was imperative that uniform test conditions be maintained. The chamber pressure recorded during the firings was an important part of the data obtained in this investigation, since it was used to indicate the degree of nozzle erosion that occurred. In order to use the recorded change in pressure as a measure of nozzle erosion, it was necessary to prevent pressure variations resulting from causes other than nozzle erosion. Therefore, the pressure transient obtained in preliminary firings of as-received propellant grains was eliminated by modifying the propellant grains in the manner described subsequently. Figure 4(b) shows the pressure traces obtained with the modified grains.

Preliminary firings indicated that the pressure transient was caused by variation of either burning rate or burning surface area with time. Analysis of the internal ballistics of solid-propellant rocket engines indicated that a suitable solution to the problem could be obtained by assuming that the burning rate was changing during the pressure transient, while the burning surface area remained constant. The general mathematical expressions (ref. 8) of the relations among burning rate, burning surface area, and chamber pressure are as follows:

$$P = \frac{Sr\rho}{A_t C_d} \tag{1}$$

where

P chamber pressure

S burning surface area

r burning rate

ρ propellant density

A_t area of nozzle throat

C_d nozzle-discharge coefficient

and

$$r = aP^n \tag{2}$$

where a and n are constants. Since A_t, C_d, and ρ are constant for a given engine configuration and propellant formulation, equation (1) can be simplified to

$$P = KSr \tag{3}$$

where K is a constant. From equation (3) it is evident that if burning rate increased during the pressure transient, a constant chamber pressure could be obtained by inversely varying burning surface area. Since the initial burning rate was lower than the equilibrium value, it obviously was necessary to increase the initial burning surface area; however, the variation of chamber pressure and burning rate must also satisfy equation (2). This was achieved by calculating the initial burning rate at equilibrium pressure. From equation (2) the following relation may be determined:

$$r_i = r_o\left(\frac{P_i}{P_o}\right)^n$$

where r_o and P_o are the initial burning rate and pressure with unaltered surface, and r_i and P_i are the initial burning rate and pressure with altered surface area. The burning rate r_o was calculated from equation (3), where P_o was measured and the burning surface area S was assumed to be the area of the grain circular end face. The initial burning rate r_i having been calculated, the burning surface area required for design pressure at the beginning of the transient period could be calculated from equation (3). Similarly, the surface area could be determined at any time during the transient period.

Pressure-transient data obtained in preliminary firings indicated that the apparent burning rate increased essentially linearly during the transient period; therefore, the grain burning surface was modified in such a manner that the initially exposed surface area was increased and during firing regressed approximately linearly to that of the grain circular end face. The modification of the grain burning area is shown in figure 5. Comparison of figures 4(a) and (b) illustrates the degree to which the pressure transient was eliminated.

Postoperation Analysis

The pressure data were used to determine the relative performance of materials as nozzles. The final chamber pressure and equation (1) described earlier in the discussion of the burning surface modification were used to calculate total erosion of each nozzle. The total erosion of each nozzle was also determined from a shadowgraph of the nozzle-throat cross section at a magnification of 20. The enlarged throat area represented by the shadowgraph was determined

by use of a planimeter. There was generally good agreement between erosion data calculated from the pressure traces and the data obtained from shadowgraphs of the nozzles. Since the calculated data agreed well with the shadowgraph results for total erosion, meaningful calculations of erosion could be made for specific time intervals during the firings. Accordingly, the average erosion rate during pressure regression from 1000 to 800 pounds per square inch was also calculated from equation (1) and from the time interval during which this pressure regression occurred. After shadowgraphs were obtained, nozzle inserts were cut in half axially for macro- and microexamination. The nozzle cavity was, in some instances, filled with epoxy resin to prevent spalling of reacted material from the inner surface during the cutting operation. One part of the nozzle was polished, examined under a low-power binocular microscope, and photographed. The half section of the nozzle was again cut axially and prepared for metallographic examination. Photomicrographs were taken of the region of the nozzle inserts near the surface exposed to the exhaust gases.

RESULTS

Rocket-Nozzle Performance

Nozzle erosion. - The chamber-pressure - time traces obtained during nozzle material-evaluation firings are shown in figure 6. Regression of chamber pressure from the design pressure of 1000 pounds per square inch provides an indication of the extent of erosion of the nozzle throat.

The erosion thus indicated varied from zero with the molybdenum nozzle (fig. 6(a)) to complete failure with the nylon-reinforced-phenolic nozzle (fig. 6(l)). The LT1B and LT2 cermet nozzles and the silicon nitride nozzle (figs. 6(b) to (d)) demonstrated only very slight pressure regression. Final pressures were 940 pounds per square inch or higher, ignoring the slight pressure rise observed just prior to conclusion of each test; however, it should be noted that these nozzles cracked during firing. This cracking will be discussed further in a later section.

Arc-cast tungsten and ZT graphite nozzles showed a greater pressure regression to 840 and 775 pounds per square inch, respectively (figs. 6(e) and (f)). Speer 3499 graphite, ATJ graphite, and the 40-percent-resin refrasil-reinforced-phenolic nozzles showed a considerable drop in pressure to approximately 500 pounds per square inch (figs. 6(g) to (i)). For these three materials, the chamber pressure decreased rapidly in the early portion of the firings from initially high pressures to a value of approximately 500 pounds per square inch. The drop occurred in 10 to 15 seconds, and for the remainder of the firing time, chamber pressure remained fairly constant, which indicated that little additional erosion of these nozzles occurred after the initial loss of material. While this performance is undesirable for high-pressure operation, it demonstrates that these materials might be satisfactory for lower-pressure operation. The 20-percent-resin phenolic-refrasil nozzle and the graphite-cloth-phenolic nozzle (figs. 6(j) and (k)) both showed results similar to the 40-percent-resin phenolic-refrasil nozzle (fig. 6(i)). Both these nozzles, however, displayed a still greater regression of pressure to less than 400 pounds per square inch during the first 10 seconds of firing. The nylon-reinforced-phenolic nozzle (fig. 6(l)) eroded almost completely in this time.

Performance of nozzle inserts with various erosion-resistance criteria is summarized in table II in the order of decreasing erosion resistance. For each nozzle material this table shows the regressed chamber pressure, the average throat-surface-erosion rate from 1000 to 800 pounds per square inch, the throat-surface erosion obtained for the entire firing (based on a circular throat), and the increase in area of the throat resulting from the firing. The relative rating of the various materials is about the same for all the erosion-resistance criteria.

Several materials demonstrated good resistance to erosion. Arc-cast molybdenum showed no measurable erosion for the entire firing. The cermet and ceramic nozzles (LT1B and LT2) and silicon nitride, showed total throat-surface erosion of 3 mils or less. These three materials failed by thermal-stress cracking, but this failure did not appear to affect their performance during the firing. The tungsten and ZT graphite nozzles eroded a total of 5 and 9.5 mils (calculated), respectively. The remaining materials showed relatively high total calculated erosion ranging from 26 mils for the 40-percent-resin phenolic-refrasil nozzle to complete disintegration of the phenolic-nylon nozzle.

Another comparison of relative nozzle-material performance indicated in table II is the average erosion rate that occurred during chamber-pressure regression from 1000 to 800 pounds per square inch. These data provide an indication of nozzle-material performance under the most severe conditions of the test. For molybdenum, tungsten, the cermet and ceramic materials, and ZT graphite, the average erosion rate was low, 0 to 0.6 mil per second. The erosion rates of the remaining nozzle materials were considerably greater at these high pressures ranging from 2.4 mils per second for Speer 3499 graphite to over 20 mils per second for phenolic nylon. It is interesting to note that although the 40-percent-resin phenolic-refrasil nozzle showed a higher erosion rate during the early part of the firing than did the two molded graphite nozzles, its total erosion was slightly lower. The lower thermal conductivity of the phenolic material would tend to cause the throat-surface region to reach a higher temperature more quickly than the higher conductivity graphite nozzles. Also the phenolic-resin materials must melt and char before reaching equilibrium. Both these factors would cause a high initial erosion rate for this material. Factors influencing the erosion resistance of these materials are discussed in the DISCUSSION OF RESULTS section.

Nozzle temperature. - Nozzle-temperature data were obtained for three materials in separate firings from thermocouples imbedded at various distances from the gas surface in the nozzle throat. Data were obtained for the molybdenum, ATJ graphite, and 40-percent-resin phenolic-refrasil nozzles (see fig. 7). The temperature indicated by thermocouples installed 0.05 inch from the gas surface reached 2540° and 2630° F for the molybdenum and graphite nozzles, respectively, in 15 seconds. Thermocouple 1 in the phenolic-refrasil nozzle failed after approximately 5 seconds before reaching maximum temperature. The temperature difference between stations 1 or 4 and 3 (fig. 7(a)) for the molybdenum nozzle was always less than 300° F. For the graphite nozzle (fig. 7(b)) this temperature difference reached a maximum of approximately 700° F when temperature equilibrium was reached. As might be expected, the phenolic-refrasil nozzle demonstrated a much greater insulating effect (fig. 7(c)). This effect was indicated by the much greater temperature difference (1700° F) between thermocouples 1 and 3 after

5 seconds of firing and by the small temperature rise of 100° and 200° indicated by thermocouples 2 and 3, respectively, after 25 seconds.

Extrapolation of the radial temperature-distribution data to obtain approximate nozzle-surface temperature for essentially equilibrium conditions indicated values of 2800° F for the ATJ graphite nozzle and 2600° F for the molybdenum nozzle. It is significant that these temperatures are considerably below the flame temperature of 4700° F.

Postfiring Nozzle Studies

Macroexamination of nozzles. - Macrophotographs of all nozzles sectioned after firing except the phenolic nylon are shown in figure 8. The arc-cast molybdenum and arc-cast tungsten nozzles are shown in figure 8(a). As previously indicated, the molybdenum nozzle did not erode, but the tungsten nozzle eroded at the nozzle throat to a depth of 5 mils. The macrophotograph indicates that nonuniform erosion occurred with the tungsten nozzle. There was no indication of a reacted layer of material along the gas surface of either material. The LT1B, LT2, and silicon nitride nozzles are shown in figure 8(b). These nozzles eroded very slightly and uniformly; however, as shown in the photographs, all three materials failed by thermal-stress cracking. The nozzles cracked extensively during firing both parallel and perpendicular to the direction of gas flow, as indicated by the oxide deposits on the crack surfaces. Although cracking occurred during firing, it did not appear to affect nozzle performance adversely. The cracks were not readily apparent until the nozzles were released from the steel sleeve and insulation by the sectioning process.

The ATJ, Speer 3499, and ZT graphite nozzles are shown in figure 8(c). The erosion of the ZT graphite nozzle was uniform, while that of the ATJ and Speer 3499 nozzles was markedly nonuniform. Again, there was no evidence of reacted material on the inner surface of the nozzles. Three of the four reinforced-phenolic nozzles are shown in figure 8(d). The fourth, a nylon-reinforced-phenolic nozzle, was so damaged during firing that it could not be prepared for examination. All the reinforced-plastic nozzles were so weakened during firing by charing and delamination along the planes of the fiber-reinforcing material that they tended to fall apart during preparation for macro- and microexamination. The 20-percent-resin phenolic-refrasil nozzle, which eroded about $1\frac{1}{2}$ times as much on an area basis as the 40-percent-resin phenolic-refrasil nozzle (table II), developed less char layer. It is interesting to note that phenolic-graphite nozzle did not develop an appreciable char layer.

Microexamination of nozzles. - Specimens of each nozzle were prepared and examined metallographically. Representative photomicrographs at various magnifications are shown in figure 9. The arc-cast molybdenum nozzle (fig. 9(a)) showed no indication of degradation or reaction other than some recrystallization along the gas surface. Since no pressure regression or erosion occurred, the absence of reaction products was to be expected. Moderately worked molybdenum can recrystallize at temperatures above 2000° F. Residual stresses introduced by machining coupled with the nozzle temperature of 2600° F could account for the re-

crystallization observed at the nozzle surface. Microphotographs of the arc-cast tungsten nozzle, which eroded slightly, are shown in figure 9(b). There is evidence of material removal from the surface, but no residue of reaction products was visible. Since some grains were pulled from the sharp outer edges of this nozzle during machining, removal of material by grain-boundary separation was suspected; however, the mechanism of material loss from the nozzle throat was clearly not one of grain-boundary separation as shown in figure 9(b). Photomicrographs of the LT2 cermet nozzle are shown in figure 9(c). Since almost negligible erosion occurred, the absence of reacted material might be expected; however, thermal-stress cracking in the throat region and a zone of dispersoid agglomeration at the surface of the nozzle throat was noted. Agglomeration apparently occurred in the otherwise evenly dispersed aluminum oxide constituent. The affected area was quite small. Almost all of the affected area was included in the photomicrograph (fig. 9(c)). Determination of possible variation in chemical composition resulting from volatilization of elements such as chromium, one of the principal alloying constituents that may have accompanied agglomeration was not attempted because of the small area visibly affected. Thermal-stress cracking of the silicon nitride nozzle is plainly visible in figure 9(d). A color change was noted in a narrow band along the entire gas surface of the nozzle as shown in the upper photomicrograph of figure 9(d). An investigation by X-ray examination of silicon nitride, which showed a similar color change (ref. 9), indicated that no phase change occurred.

DISCUSSION OF RESULTS

Failure Mechanisms

The failure mechanisms of nozzle materials were categorized into four main types in the following discussions: thermal-stress cracking and three distinct erosion mechanisms, melting or sublimation, oxidation, and mechanical erosion or abrasion.

When direct evidence of these failure mechanisms was not found, as was true for several materials, indirect evidence was used to establish the probable failure mechanism.

Refractory metals. - The refractory metals, molybdenum and tungsten, demonstrated the best overall performance of all the materials tested. Molybdenum showed no evidence of material loss (table II). Since molybdenum has relatively poor elevated-temperature oxidation resistance in air, material loss by oxidation in the propellant exhaust gases might be expected; however, the molybdenum nozzle was completely unaffected by the exhaust products. Neither molybdenum nor tungsten showed any tendency to crack as the result of thermal stress.

Consideration of the various mechanisms by which erosion may have occurred in the tungsten nozzle indicated that oxidation was probably responsible. For example, melting could not have occurred because the propellant flame temperature, 4700° F, was well below the melting point of tungsten. Also the observed temperatures for the molybdenum nozzle were less than 3000° F, and the tungsten-nozzle temperatures were probably similar. Mechanical erosion seemed unlikely, since tungsten is stronger than molybdenum at the observed nozzle temperatures

and no material removal occurred in the molybdenum nozzle. The poor cohesive strength of the grains of arc-cast tungsten indicated earlier by loss of grains during machining might suggest that erosion resulted from loss of complete grains at the nozzle throat; however, macro- and microexamination of the tested nozzle indicated that no grains were pulled from the surface during firing. Rather, as indicated in figure 9(b), the material at the tungsten-nozzle throat surface appeared to have been removed uniformly by oxidation. There was no evidence of preferential attack at the grain boundaries. Since no reaction products were detected on the nozzle surface after firing, it was not possible to determine the exact nature of the oxidation reaction that occurred.

Graphites. - All three graphite materials eroded, as indicated in table II. The molded graphites, ATJ and Speer 3499, showed about the same total erosion. Both materials eroded considerably more than the recrystallized high-density ZT graphite. As in the case of tungsten, no positive indication of failure mechanisms was evident in postfiring examination; however, possible failure mechanisms are suggested by comparing the variation of nozzle erosion with known variations of physical properties of the two types of graphite. Since the sublimation temperature for both types of graphite is similar (approx. 6700° F) and since the nozzle surface temperatures were less than 3000° F, it is unlikely that sublimation of the graphites was an important failure mechanism.

Graphites in general are susceptible to oxidation and have low strength at the nozzle operating temperatures of interest (ref. 10). Hence, it is possible that both oxidation and mechanical erosion were active in causing material loss.

The ZT graphite is both stronger (ref. 11) and more resistant to oxidation because of its higher density. Oxidation rates measured by weight change in slow-moving air at temperatures from 1100° to 2200° F are essentially the same for ATJ and ZT graphite. (This information was obtained in private communication with Dr. L. M. Litz of Parma Research Center of the National Carbon Co.) However, since the ZT graphite had a density of 1.90 grams per cubic centimeter compared with 1.72 grams per cubic centimeter for ATJ, there would be less volume of ZT graphite material affected. This variation of density could account for about a 10-percent greater depth of material loss for the ATJ graphite for the preceding test conditions. Also, preferential oxidation of the binder material occurs with ZT and ATJ graphites but would probably be more pronounced with the ATJ graphite. (This information also was obtained from Dr. L. M. Litz of the National Carbon Co.) This preferential attack of the binder produces a roughened surface. If it is assumed that the oxidation of the graphites in the rocket engine parallels that observed in air, the roughened surface would be expected to result in increased mechanical erosion. Therefore, the greater depth of oxidation was a principal mechanism in the removal of material with both the molded and recrystallized graphite nozzles. Mechanical erosion was probably an additional failure mechanism that was more pronounced with the molded-graphite nozzles.

Cermets and ceramic. - Although the LT1B, LT2, and silicon nitride nozzles eroded only very slightly in this investigation, they probably would not operate

satisfactorily at much higher temperatures or for longer times. For example, melting of LT1B and LT2 and sublimation of silicon nitride occur at temperatures ranging from 3100° to 3500° F (refs. 12 and 13). Estimates based on material properties and measured nozzle temperatures of other materials indicate that the nozzle-surface temperatures of the two cermet nozzles and the silicon nitride nozzle were probably about 2800° F with the 4700° F flame temperature used in this investigation. For this reason, little increase in propellant flame temperature could be tolerated by these materials. In fact, there was some evidence of initial degradation of the LT2 nozzle in this investigation, as indicated by agglomeration of the aluminum oxide dispersoid in this material (fig. 9(c)).

It was indicated earlier that the LT1B, LT2, and silicon nitride nozzles cracked extensively as a result of thermal shock (fig. 8(b)). Since the thermal stresses in the small nozzles of this investigation are probably lower than those of full-scale nozzles, the results obtained with the cermet and ceramic nozzles indicate possible limitations of such materials for full-scale rocket applications.

Composite materials. - All four reinforced-phenolic-resin nozzles eroded drastically during the initial high-pressure portion of the firings. The rate of erosion or material loss diminished as lower chamber-pressure levels were reached. This behavior might be expected for these nozzles where material removal occurred by ablation. The ablation process normally provides heat protection by melting and vaporization of the resin and the reinforcement material. When a glassy reinforcement material such as refrasil is melted, a viscous layer is formed on the surface. This liquid layer is partially vaporized, while the remainder is mechanically removed by the flowing gas stream. The efficiency of heat absorption by this ablation process is primarily a function of the stagnation enthalpy at the boundary layer and the stagnation pressure (refs. 14 and 15). The heat-absorption or ablation efficiency increases with increasing enthalpy and decreasing pressure. Thus, as ablation occurs and the nozzle-throat area increases, the chamber pressure decreases, and the heat-absorption efficiency improves. As a result of the increased heat-absorption efficiency, the rate of material removal would be reduced. Furthermore, the decrease in heat-transfer coefficient and accompanying heat flux resulting from the lower pressure would also tend to reduce the rate of material removal.

The relatively poor performance of the graphite-cloth-reinforced-phenolic nozzle compared with that of the refrasil-phenolic nozzles apparently resulted from the fact that the graphite-reinforcing fibers have a higher conductivity than the refrasil fibers. More rapid conduction of heat from the surface into the bulk material of the graphite-reinforced nozzles would prevent the surface from quickly reaching the high temperatures necessary for efficient ablation cooling. This reasoning is supported by the lack of a marked char-layer formation (fig. 8(d)).

Comparison of Thermal Stress in Small and Large Nozzles

The thermal-shock resistance of nozzle materials is of major importance in the design of full-scale rocket engines. Since the heat flux in rocket nozzles is severe, the usefulness of many temperature-resistant materials may be limited

by their susceptibility to thermal-shock failure. For this reason, in evaluating materials in small-scale engines, it is desirable to know the relative severity of the thermal stresses in the small nozzle compared with those of typical full-scale nozzles.

The magnitude of the thermal stresses induced in a rocket nozzle of a given material is affected by such factors as diameter, wall thickness, nozzle shape, axial and radial temperature distributions, external loading, and end restraints. As a result of this complexity and the differences in geometry and installation configuration of various nozzles, exact determination of thermal stress is difficult; however, it is believed that simplified analyses that consider only diameter, wall thickness, and radial temperature distributions can provide an approximation of the relative severity of thermal stress in full-scale and small-scale nozzles.

An analysis was made, therefore, to determine the relative magnitude of the thermal stresses in the small-scale nozzle of this investigation (0.289-in. throat diameter with 0.45-in. wall thickness) and those in a large nozzle with an 8-inch throat diameter and an 0.8-inch wall thickness. The dimensions of the large nozzle are similar to those of some nozzles currently in use. This analysis was made by using the simplified geometry of long circular cylinders to represent nozzles and the method described in reference 16. Tangential thermal stresses were calculated from the following equation:

$$\sigma_s = \frac{E\alpha}{1 - \mu}\left(\frac{2}{b^2 - a^2}\int Tr\,dr - T_s\right)$$

where

σ_s tangential surface stress

E elastic modulus

α thermal-expansion coefficient

μ Poisson's ratio

b outer radius

a inner radius

T temperature

r radius

T_s surface temperature

The temperature distribution used for the large nozzle was calculated from the method and curves of reference 7 and the physical properties of tungsten. Since a measured temperature distribution was available for the molybdenum nozzle of

this investigation (fig. 7(c)) and since the thermal diffusivity of molybdenum is not greatly different from that of tungsten, the measured distribution was used in the stress calculations for the small nozzle. For both nozzles, the elastic modulus and the thermal-expansion coefficient of tungsten were used. The calculated stresses at the inner and the outer surfaces of the large nozzle were -159,000 and +77,000 pounds per square inch, respectively, while the corresponding stresses for the small nozzle were -73,000 and +11,000 pounds per square inch. It should again be emphasized that these calculations are based on simplified configurations. Nevertheless, it may be concluded that the calculated stress values indicate the relative difference in stress between the large and the small nozzles selected. From these calculations, it appears that the thermal stresses induced in the small nozzle of this investigation are lower than those that would occur in a typical large nozzle. Accordingly, nozzle materials that fail as a result of thermal shock in the small-scale test of this investigation probably would not be suitable for application in full-scale nozzles where the stresses would probably be higher. Thus, materials similar to LT2, LT1B, and silicon nitride, which cracked extensively in the small-scale test, would probably require some type of reinforcement such as metal honeycombs or fibers to perform satisfactorily in large nozzles.

SUMMARY OF RESULTS

A small-scale end-burning solid-propellant rocket-engine test facility to study uncooled rocket-nozzle insert materials under carefully controlled conditions has been constructed, and 12 different materials have been investigated. A nonaluminized propellant, Arcite 368, with a theoretical flame temperature of 4700° F was used. The design conditions for the engine were a chamber pressure of 1000 pounds per square inch for a 30-second firing using a nominal nozzle-throat diameter of 0.289 inch. The following results were obtained:

1. All the materials investigated, except molybdenum, eroded to some degree. Generally, the cermet and ceramic materials showed negligible erosion but cracked extensively. Tungsten and ZT graphite eroded moderately, while the molded graphites and the reinforced-phenolic materials eroded drastically.

2. Thermal-stress cracking was observed only in the cermet and ceramic materials (LT1B and LT2, and silicon nitride). The cracks extended completely through the nozzle wall in both radial and axial directions. Calculations utilizing methods based on simplified cylindrical configurations indicated that the thermal stresses in the small nozzle of this investigation were less than those in a typical full-scale nozzle. Consequently, brittle materials such as the cermets and silicon nitride would probably be unsuitable for application to a large-scale nozzle unless some form of reinforcement such as metal honeycomb or fibers were used.

3. Not only was material not removed from the molybdenum nozzle during firing, but no evidence of material reaction with exhaust gases was noted in postfiring examinations.

4. The cermet nozzles (LT1B and LT2) and the silicon nitride nozzle showed a total throat-surface erosion of 3 mils or less. Postfiring metallurgical

studies indicated agglomeration of aluminum oxide particles in the LT2 nozzle. This agglomeration is indicative of material deterioration that may lead to erosion with longer firing times or higher flame temperatures.

5. Arc-cast tungsten and high-density ZT graphite showed a total throat-surface erosion of 5 and 9.5 mils, respectively. Although no reaction products were visible on the throat surfaces after firing, it is believed that oxidation occurred, which caused removal of material in both cases. A mechanical erosion mechanism was also probably active in removing material from the ZT graphite nozzle.

6. Molded graphite nozzles, ATJ and Speer 3499, eroded extensively with a throat-surface erosion of about 30 mils. This erosion was attributed to oxidation coupled with mechanical erosion. The lower strength and the increased preferential oxidation of the molded graphites compared with ZT graphite apparently resulted in considerably more mechanical erosion with these materials than was observed with the ZT graphite.

7. Of the fiber-reinforced-phenolic nozzles, the phenolic refrasil with 40-percent-resin content showed the greatest erosion resistance. Its performance was about the same as that of the molded-graphite nozzles. The 20-percent-resin phenolic-refrasil nozzle eroded about $1\frac{1}{2}$ times as much and the graphite-cloth-phenolic nozzle eroded about two times as much as the 40-percent-resin material. The nylon-reinforced-phenolic nozzle failed catastrophically in a few seconds. Delamination of the nozzles was evident in all cases with these materials.

8. Temperatures of 2540° and 2630° F for molybdenum and ATJ graphite nozzles, respectively, were obtained from thermocouples installed 0.05 inch beneath the throat gas surface. Extrapolation of temperature data indicated that the throat-surface temperature was less than 3000° F in both instances, which is considerably below the 4700° F flame temperature of this propellant.

CONCLUDING REMARKS

An interesting systematic technique was developed in this investigation to prevent chamber-pressure variations resulting from transient burning conditions. This technique involved the use of internal ballistic formulas and preliminary firing data to determine the modification of propellant burning surface area necessary to provide a constant chamber pressure. The successful application of this method suggests that it may also be useful in varying the chamber pressure or thrust of a rocket engine in a controlled manner.

Lewis Research Center
National Aeronautics and Space Administration
Cleveland, Ohio, November 15, 1962

REFERENCES

1. Anon.: Report on Materials for Large Solid Propellant Rocket Motors of the Materials Advisory Board. Rep. MAB-150-M, Nat. Res. Council, June 12, 1959.

2. Farber, Milton: Fluorine Solid Propellants. Astronautics, vol. 5, no. 8, Aug. 1960, pp. 34;40.

3. Shulze, Charles E., Saulino, Frank A., Maccalous, Joseph W., and Emmons, Howard W.: Development and Evaluation of Materials for High Temperature Applications. The Carborundum Co., Aug. 1, 1958.

4. Lynch, J. F., Harp, J. L., and Duckworth, W. H.: Evaluation of Ceramic Materials in a Small Laboratory Rocket Motor. TR 57-3, WADC, June 1957.

5. Allen, John M., and Harp, James L.: Development of Testing Procedures and Evaluation of Refractory Materials. TR 58-682, WADC, Aug. 1958.

6. Anon.: Graphite-Based Materials for High Temperature Applications. Prog. Rep. 6, National Carbon Co., Oct. 1957.

7. Hatch, James E., Schacht, Ralph L., Albers, Lynn U., and Saper, Paul G.: Graphical Presentation of Difference Solutions for Transient Radial Heat Conduction in Hollow Cylinders with Heat Transfer at the Inner Radius and Finite Slabs with Heat Transfer at One Boundary. NASA TR R-56, 1960.

8. Lancaster, O. E., ed.: Jet Propulsion Engines. Vol. XII. Princeton Univ. Press, 1959, pp. 544-547.

9. Lynch, J. F., Bowers, D. J., and Duckworth, W. H.: Investigation of Nozzle-Failure Mechanisms in Solid-Propellant Rockets. Fourth Quarterly Prog. Rep., Battelle Memorial Inst., May 27, 1960.

10. Kennedy, A. J.: Graphite as a Structural Material in Conditions of High Thermal Flux. Rep. 121, College of Aero. (Cranfield), Nov. 1959.

11. Stroup, R. C.: New Carbon and Graphite Materials. Advanced Materials Lab., National Carbon Co., Nov. 14, 1960.

12. Anon.: Data Folder - Haynes Stellite Metal Ceramics. Haynes Stellite Co., July 1959.

13. Anon.: Data Folder - Silicon Nitride. Haynes Stellite Co., Nov. 1960.

14. Schmidt, Donald L., and Peterson, George P.: Reinforced Plastics at Very High Temperatures. TR 60-380, WADD, June 1960.

15. Adams, Mac C.: Recent Advances in Ablation. ARS Jour., vol. 29, no. 9, Sept. 1959, pp. 625-632.

16. Timoshenko, S., and Goodier, J. N.: Theory of Elasticity. Second ed., McGraw-Hill Book Co., Inc., 1951, pp. 408-412.

TABLE I. - NOZZLE MATERIALS

Class	Material	Fabrication	Source
Refractory metal	Molybdenum	Arc cast	Climax Molybdenum Co.
	Tungsten	Arc cast	Lewis Research Center
Cermet and ceramic	LT1B (59 percent Cr, 19 percent Al_2O_3, 20 percent Mo, 2 percent TiO_2)	Slipcast and sintered	Haynes Stellite Co.
	LT2 (60 percent W, 25 percent Cr, 15 percent Al_2O_3)	↓	↓
	Silicon nitride	↓	↓
Graphite	ATJ	Molded	National Carbon Co.
	Speer 3499	Molded	Speer Carbon Co.
	ZT	Molded and recrystallized	National Carbon Co.
Fiber-reinforced plastic	Phenolic refrasil (40-percent resin)	Molded	Goodyear Aircraft Corp.
	Phenolic refrasil (20-percent resin)	↓	↓
	Phenolic graphite	↓	↓
	Phenolic nylon	↓	Narmco Industries

TABLE II. - PERFORMANCE OF MATERIALS AS NOZZLES

Material	Regressed chamber pressure, lb/sq in.	Average erosion rate, from 1000 to 800 lb/sq in., mils/sec	Throat-surface erosion[a], mils		Throat-area increase, percent	
			Calculated	Measured	Calculated	Measured
Molybdenum (arc cast)	1000	[b]0	0	0	0	0
LT1B	940	[b].04 cracked	1.0	< 0.5	1.5	< 0.5
LT2	950	[b].08 cracked	2.0	0.5	3.0	0.5
Silicon nitride	980	[b].02 cracked	1.5	3.0	1.0	3.5
Tungsten (arc cast)	840	[b].2	5.0	7.5	7.0	10.5
ZT graphite	775	.6	9.5	9.0	13.5	13.0
Speer 3499 graphite	460	2.4	30.5	29.5	46.5	45.0
ATJ graphite	470	3.0	30.5	28.5	47.0	44.0
Phenolic refrasil (40-percent resin)	525	3.6	26.0	23.0	39.0	34.0
Phenolic refrasil (20-percent resin)	390	4.1	43.5	36.5	69.5	56.5
Phenolic graphite	280	6.2	54.0	63.0	89.0	106.5
Phenolic nylon	~20	> 20.0	(c)	(c)	(c)	(c)

[a]Based on a circular throat.
[b]Pressure never regressed to 800 pounds per square inch.
[c]Complete failure of nozzle.

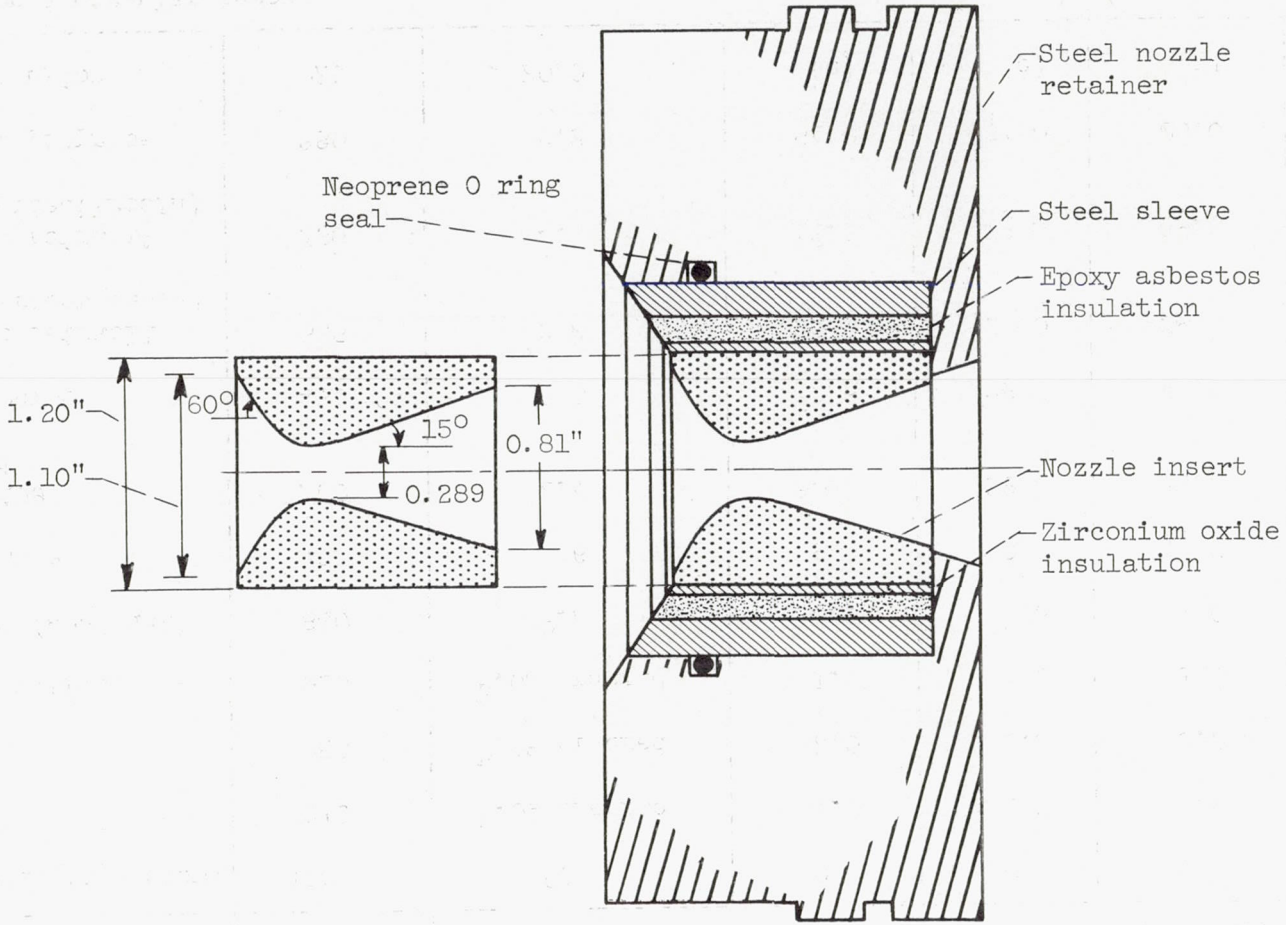

Figure 1. - Nozzle retainer and insert assembly.

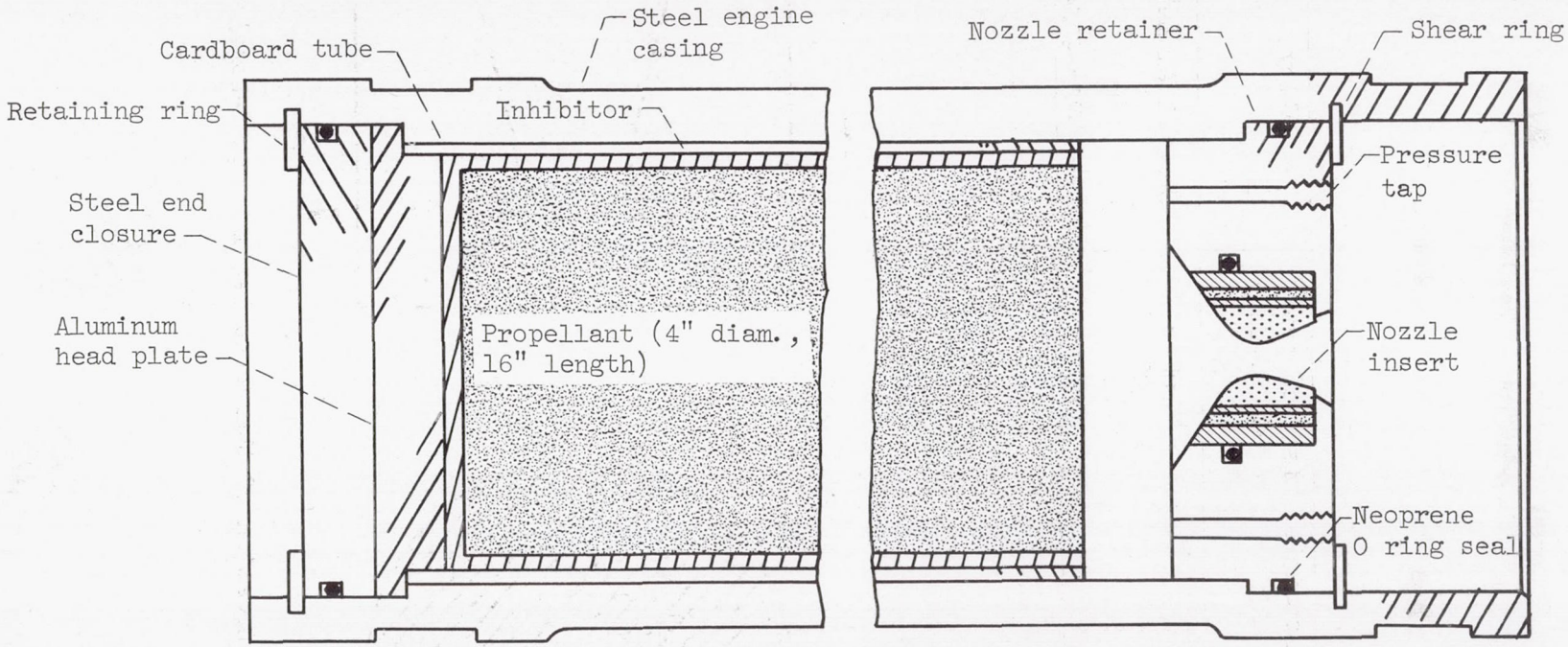

Figure 2. - Rocket engine and propellant grain assembly.

Thermocouple	Distance from throat surface, D, in.	Alloy
1	0.05	Chromel-Alumel
2	.22	↓
3	.40	↓
4	.05	Molybdenum-tungsten

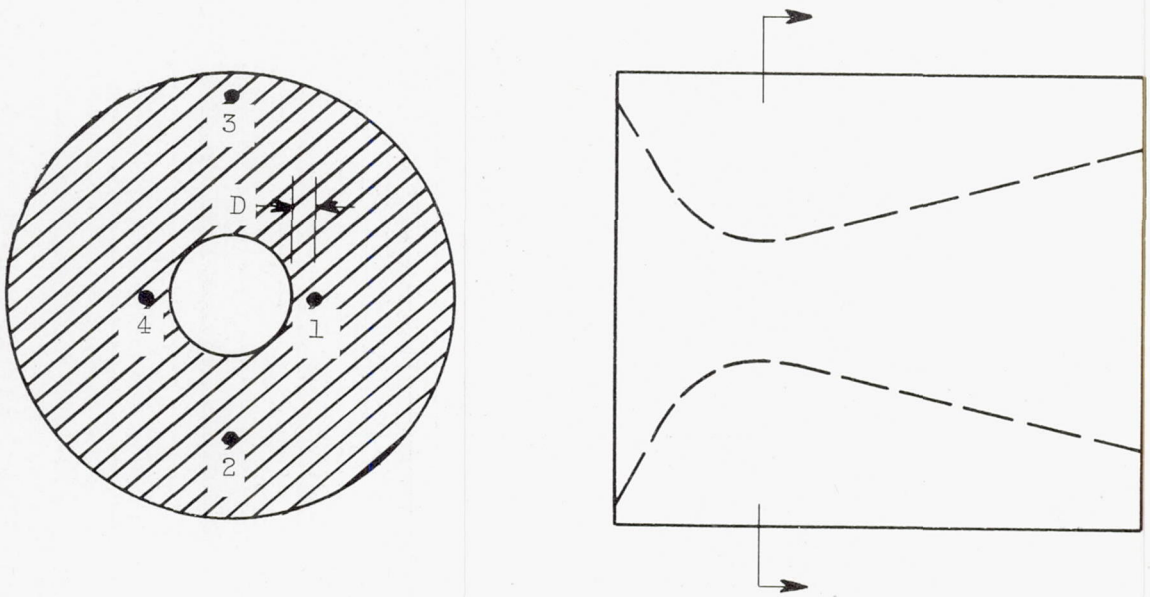

Figure 3. - Location of thermocouples in rocket-nozzle insert.

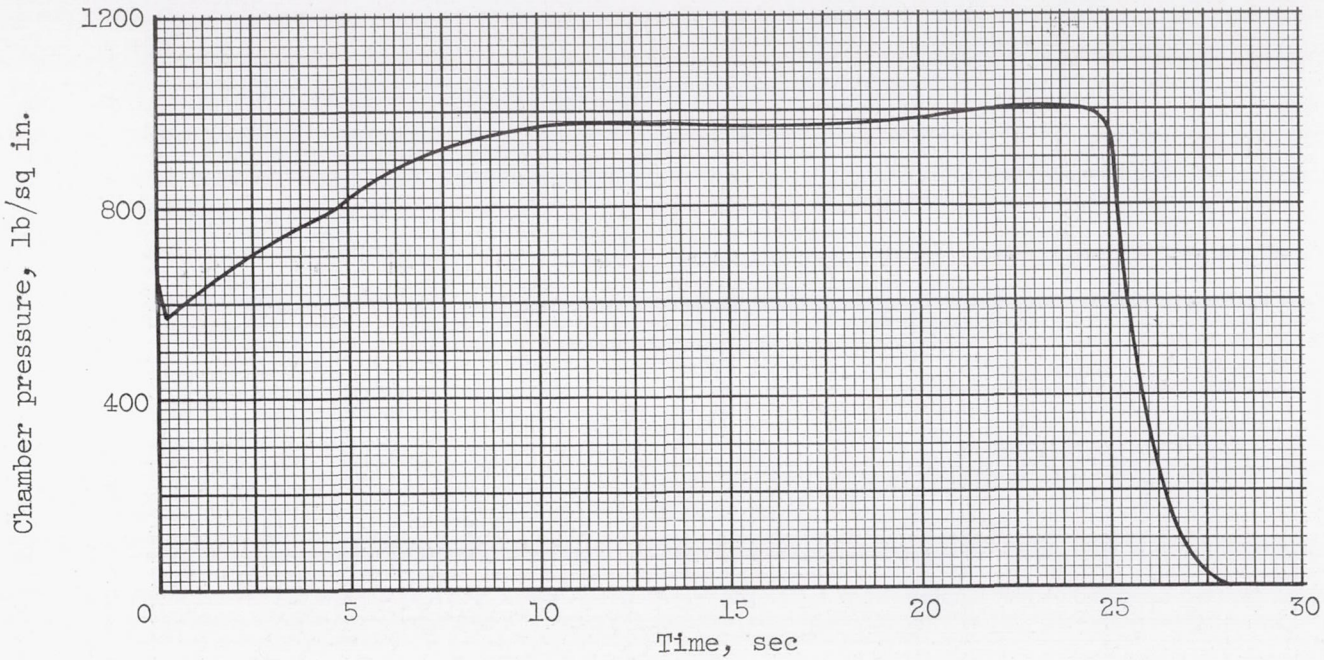

(a) As-received propellant grains.

Figure 4. - Chamber-pressure - time traces.

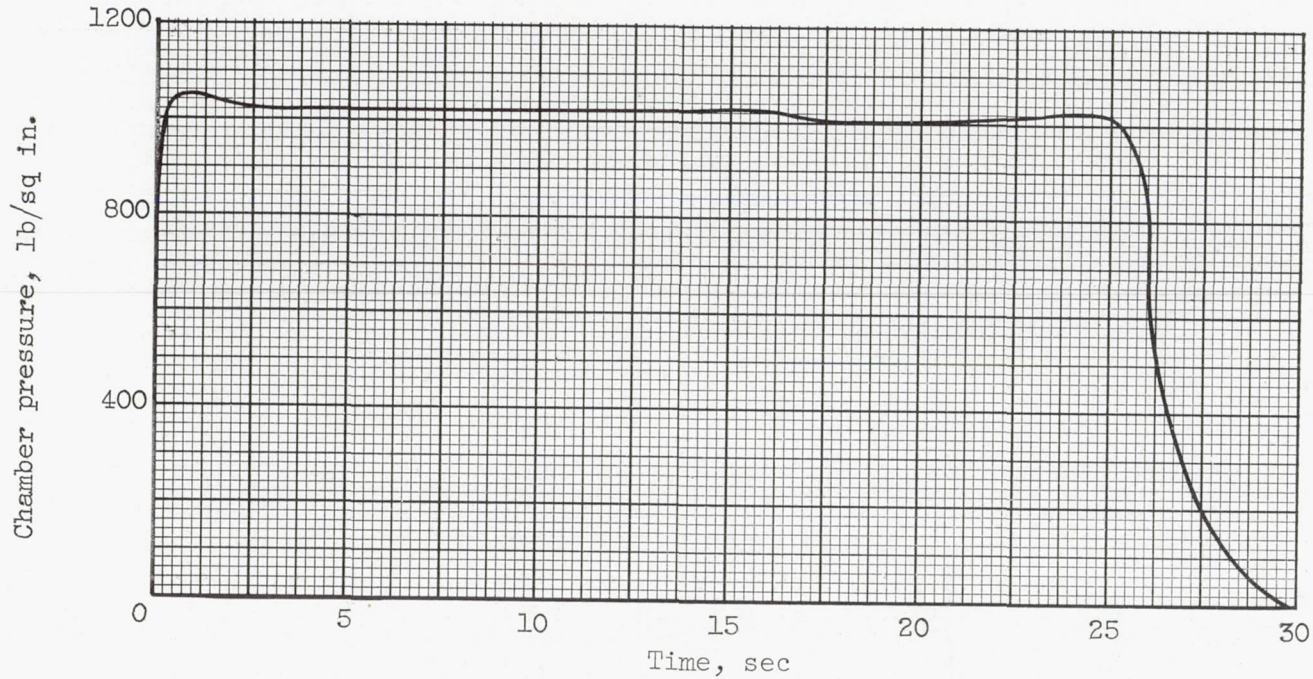

(b) Modified propellant grains.

Figure 4. - Concluded. Chamber-pressure - time traces.

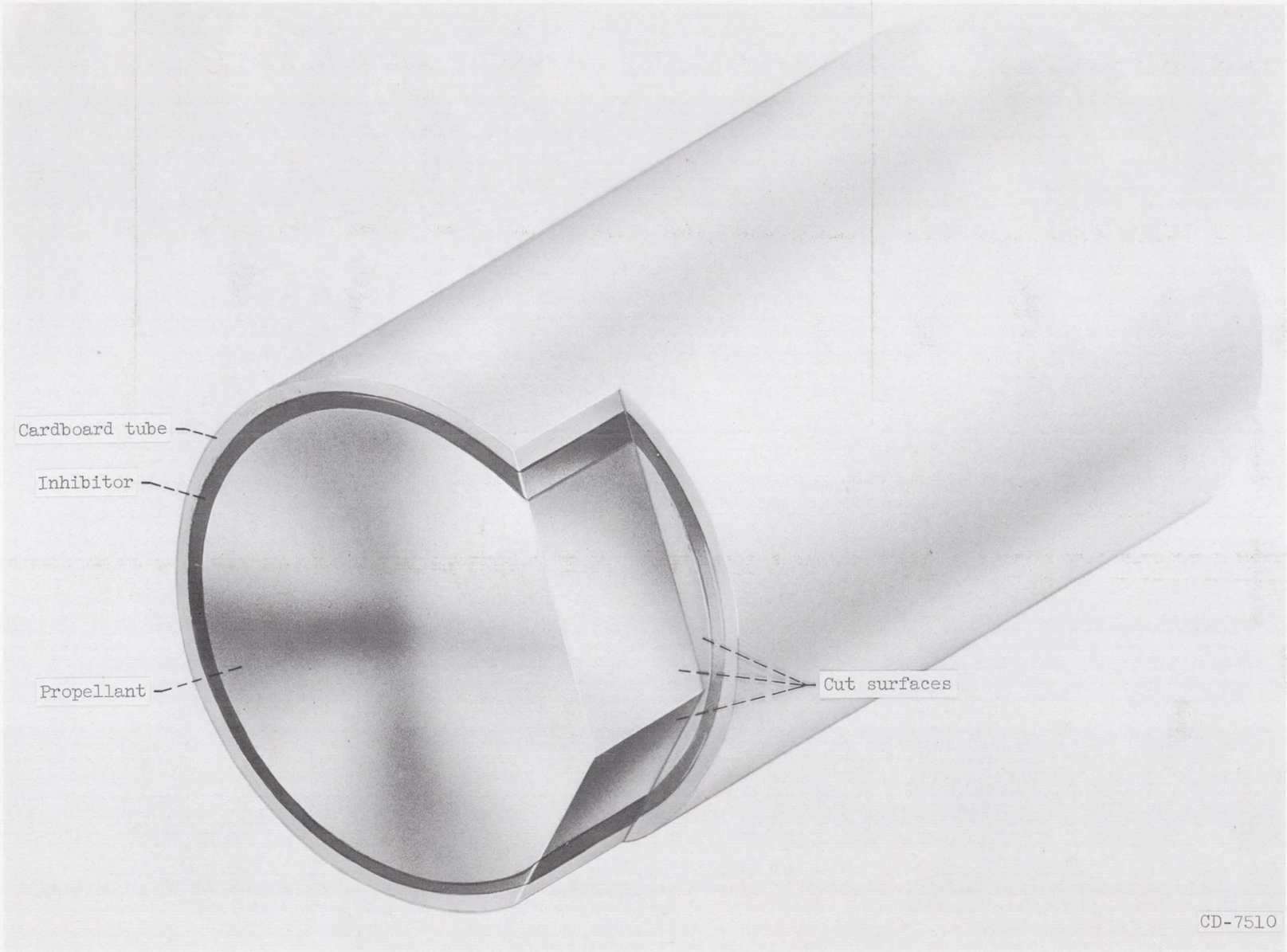

Figure 5. - Modification of propellant-grain ignition surface.

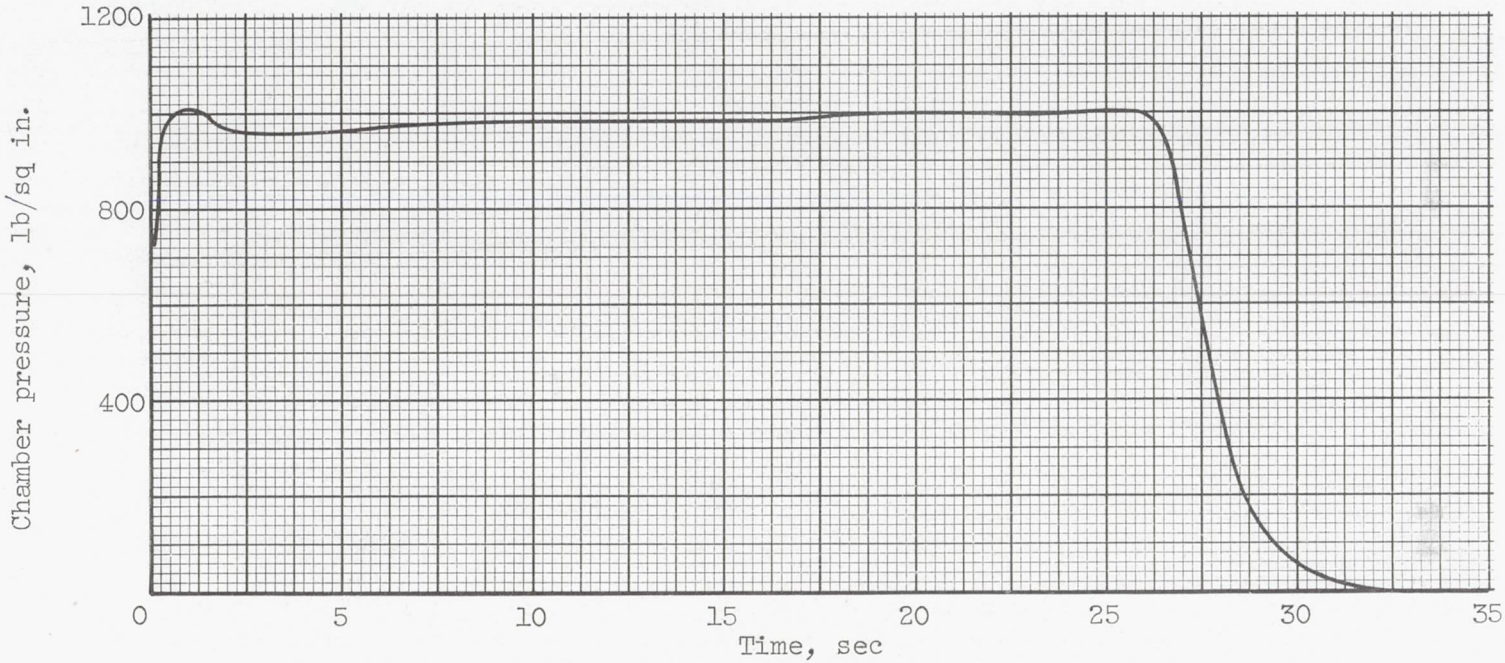

(a) Molybdenum nozzle.

Figure 6. - Chamber-pressure - time traces obtained during material-evaluation firings.

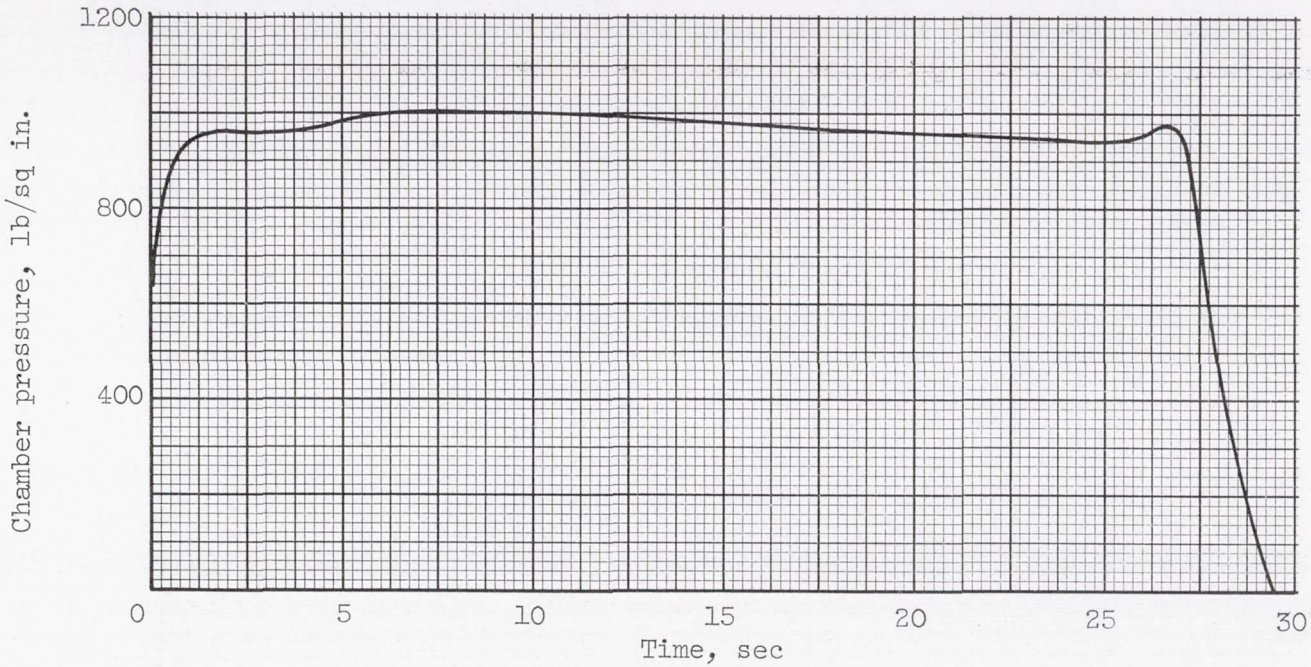

(b) LT1B cermet nozzle.

Figure 6. - Continued. Chamber-pressure - time traces obtained during material-evaluation firings.

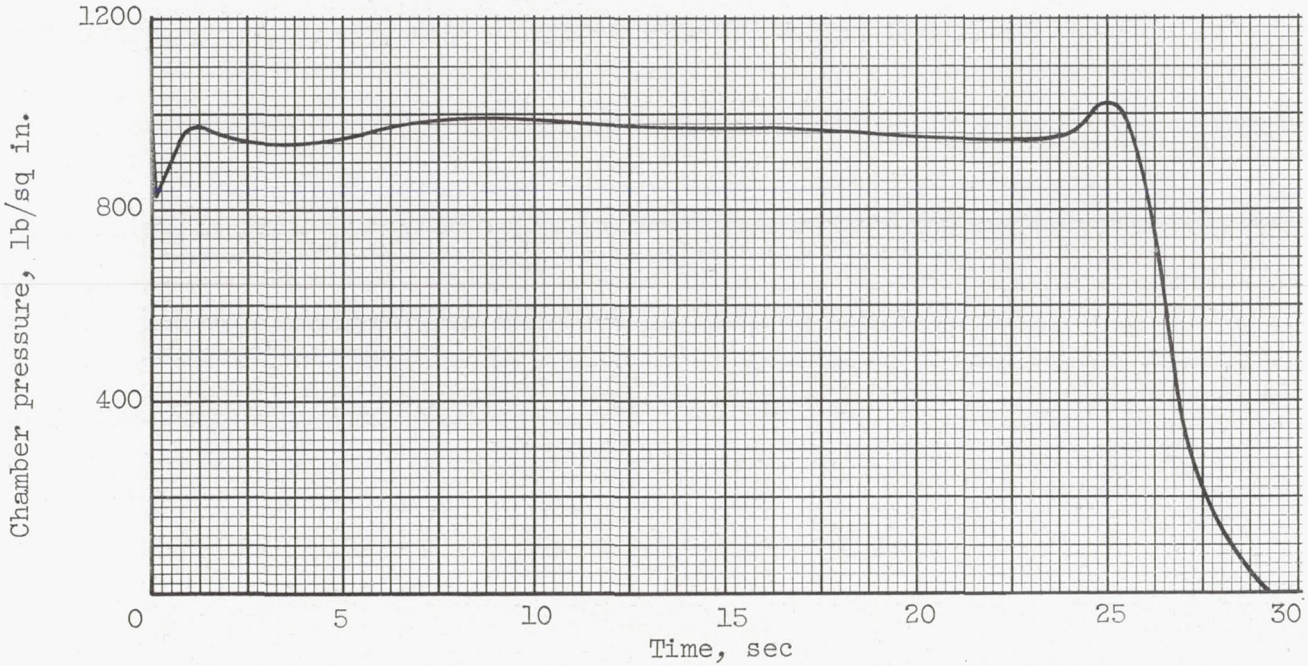

(c) LT2 cermet nozzle.

Figure 6. - Continued. Chamber-pressure - time traces obtained during material-evaluation firings.

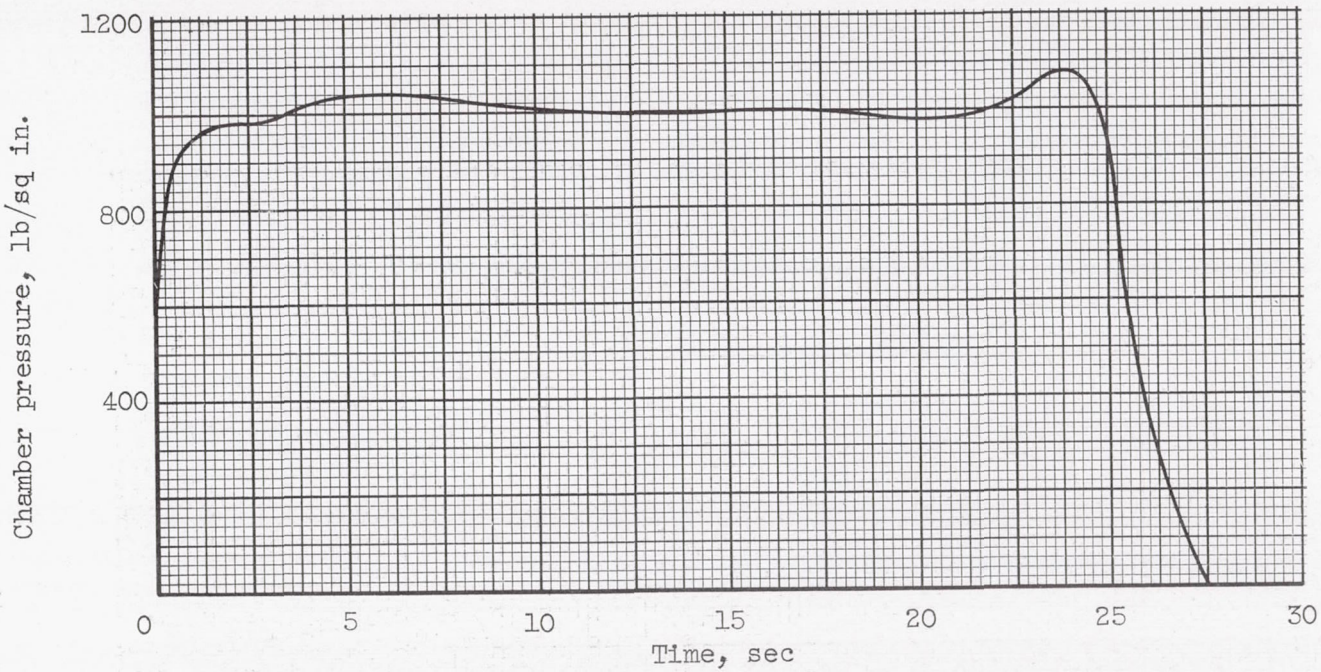

(d) Silicon nitride nozzle.

Figure 6. - Continued. Chamber-pressure - time traces obtained during material-evaluation firings.

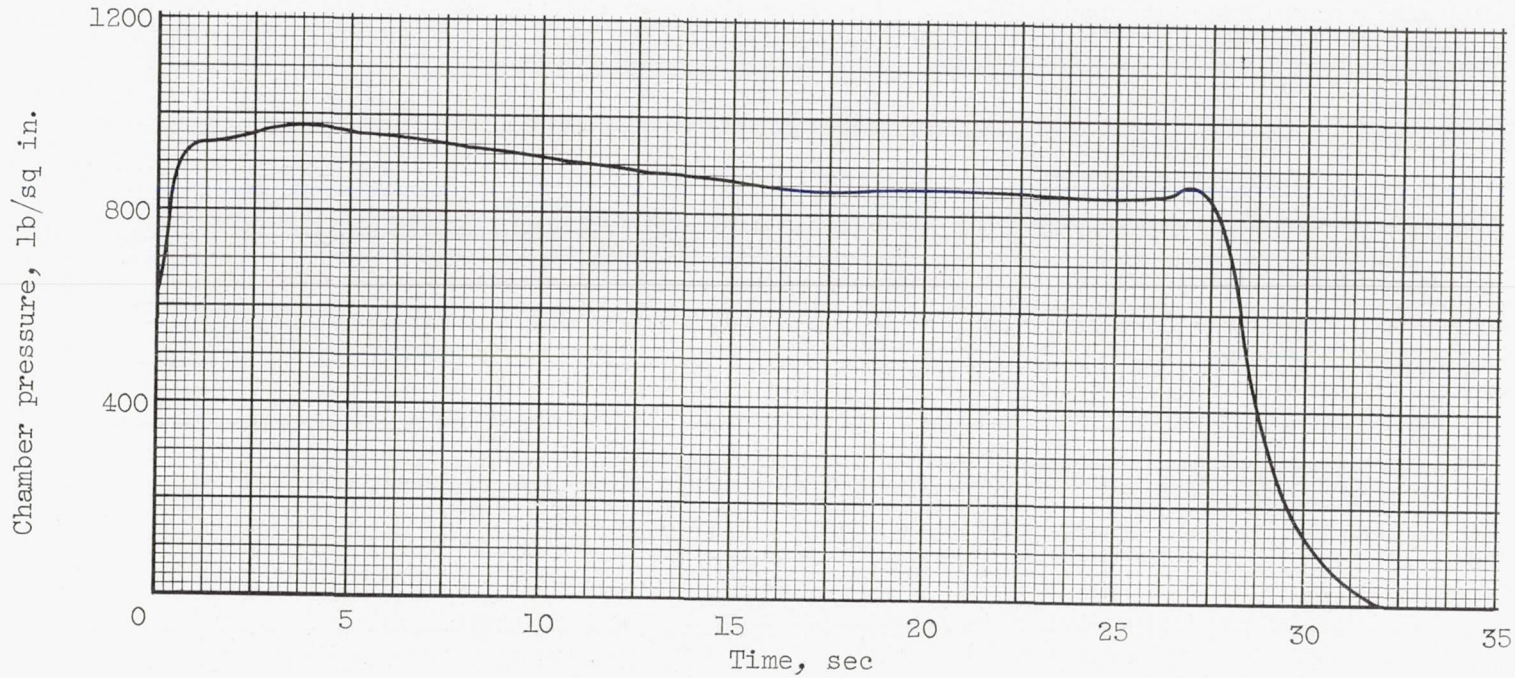

(e) Arc-cast tungsten nozzle.

Figure 6. - Continued. Chamber-pressure - time traces obtained during material-evaluation firings.

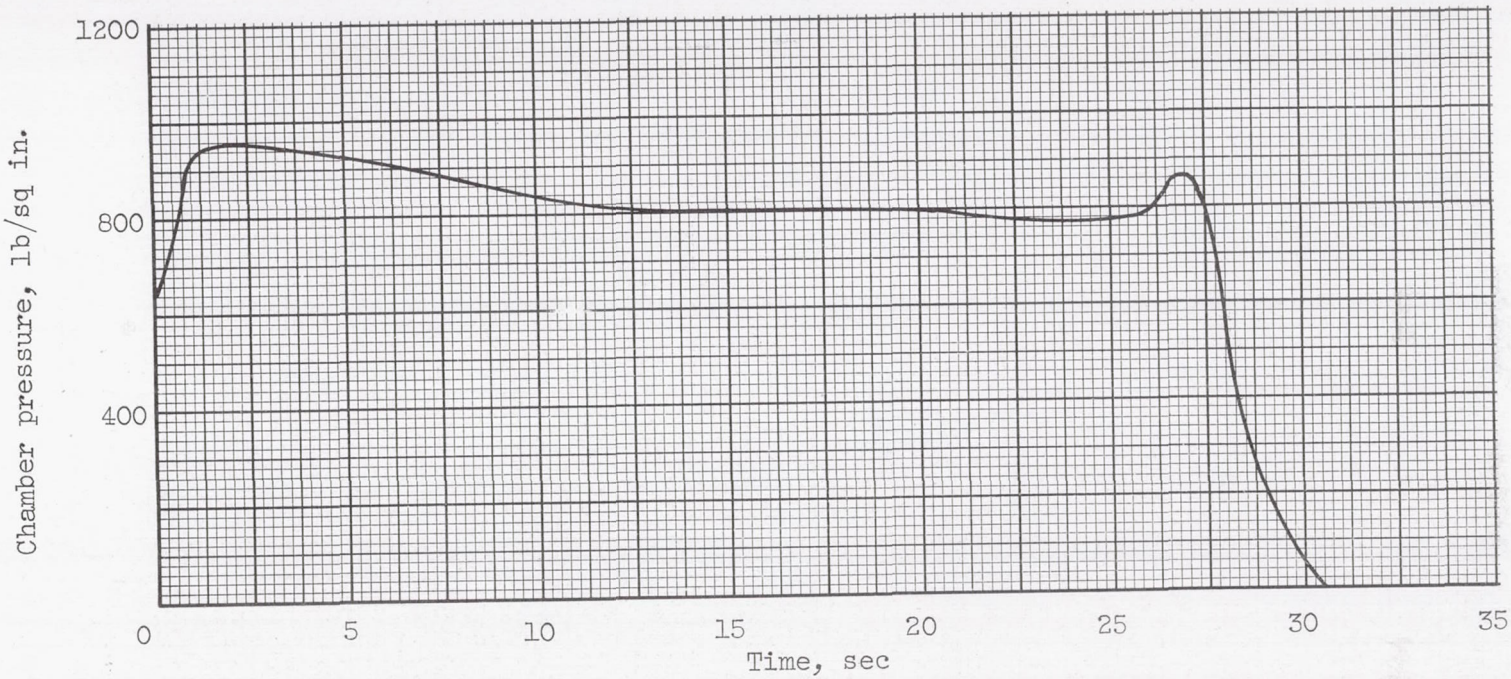

(f) ZT graphite nozzle.

Figure 6. - Continued. Chamber-pressure - time traces obtained during material-evaluation firings.

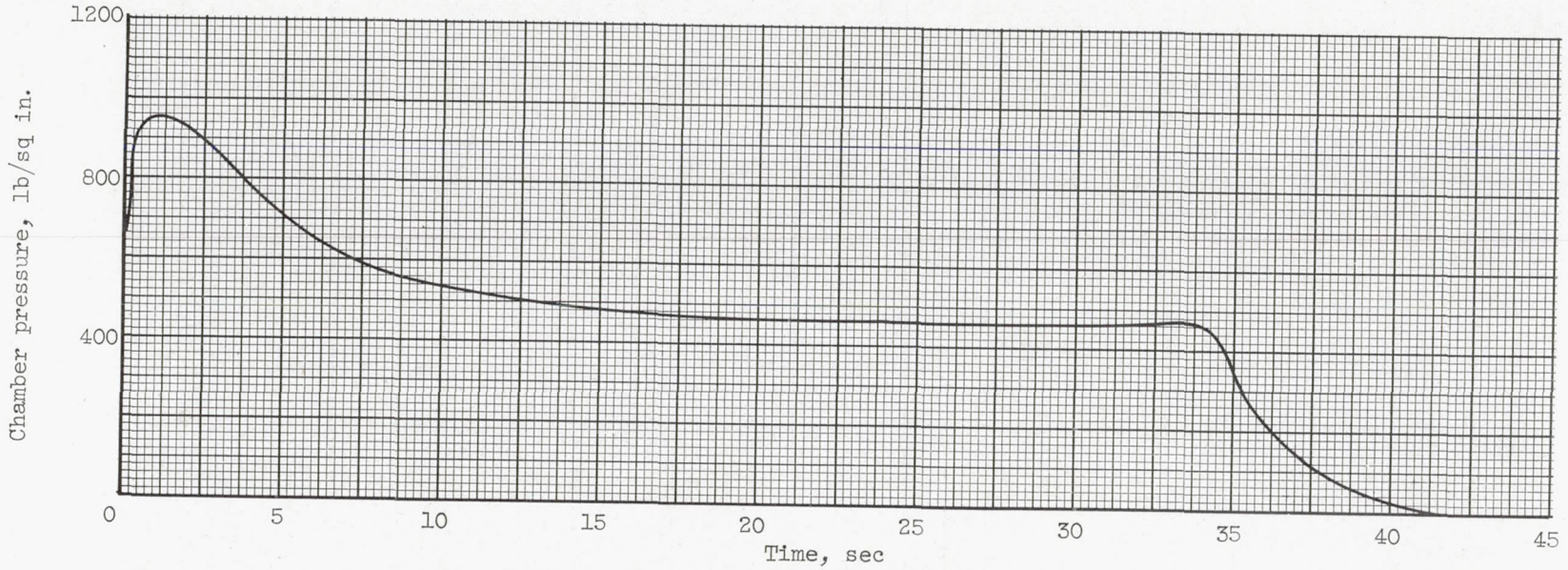

(g) Speer 3499 graphite nozzle.

Figure 6. - Continued. Chamber-pressure - time traces obtained during material-evaluation firings.

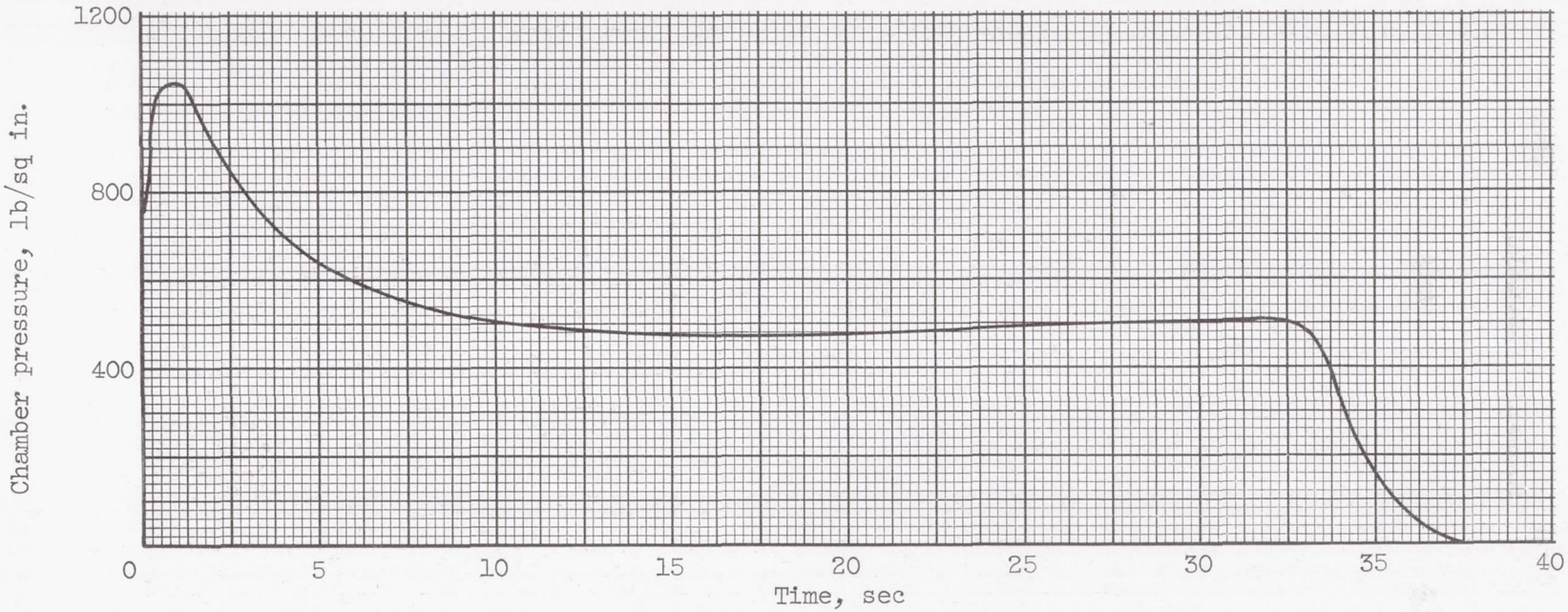

(h) ATJ graphite nozzle.

Figure 6. - Continued. Chamber-pressure - time traces obtained during material-evaluation firings.

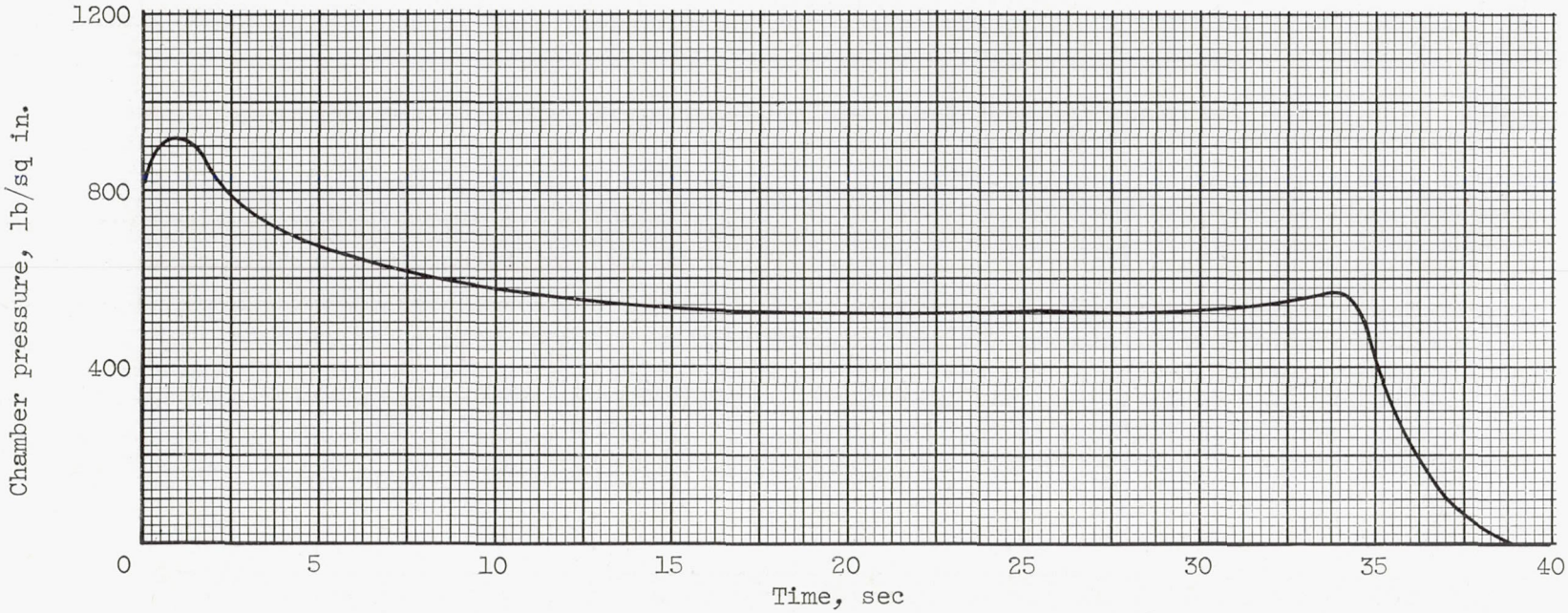

(i) Phenolic-refrasil (40-percent resin) nozzle.

Figure 6. - Continued. Chamber-pressure - time traces obtained during material-evaluation firings.

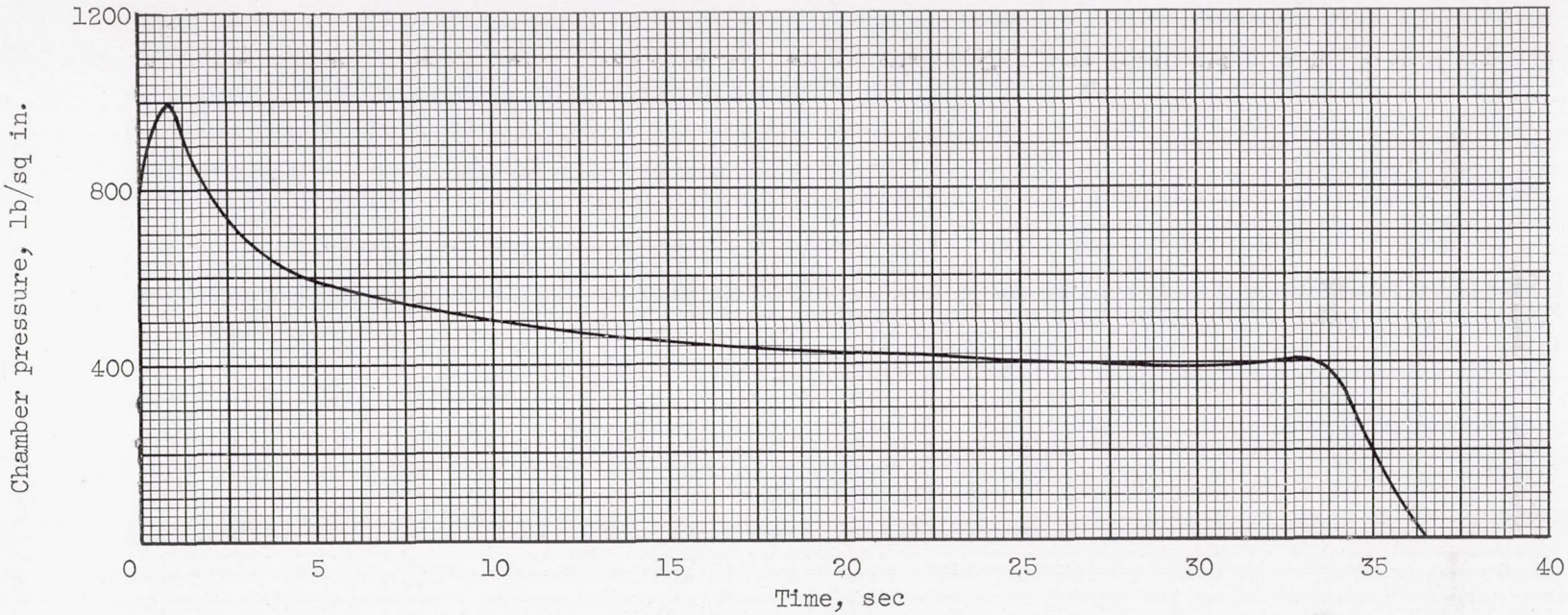

(j) Phenolic-refrasil (20-percent resin) nozzle.

Figure 6. - Continued. Chamber-pressure - time traces obtained during material-evaluation firings.

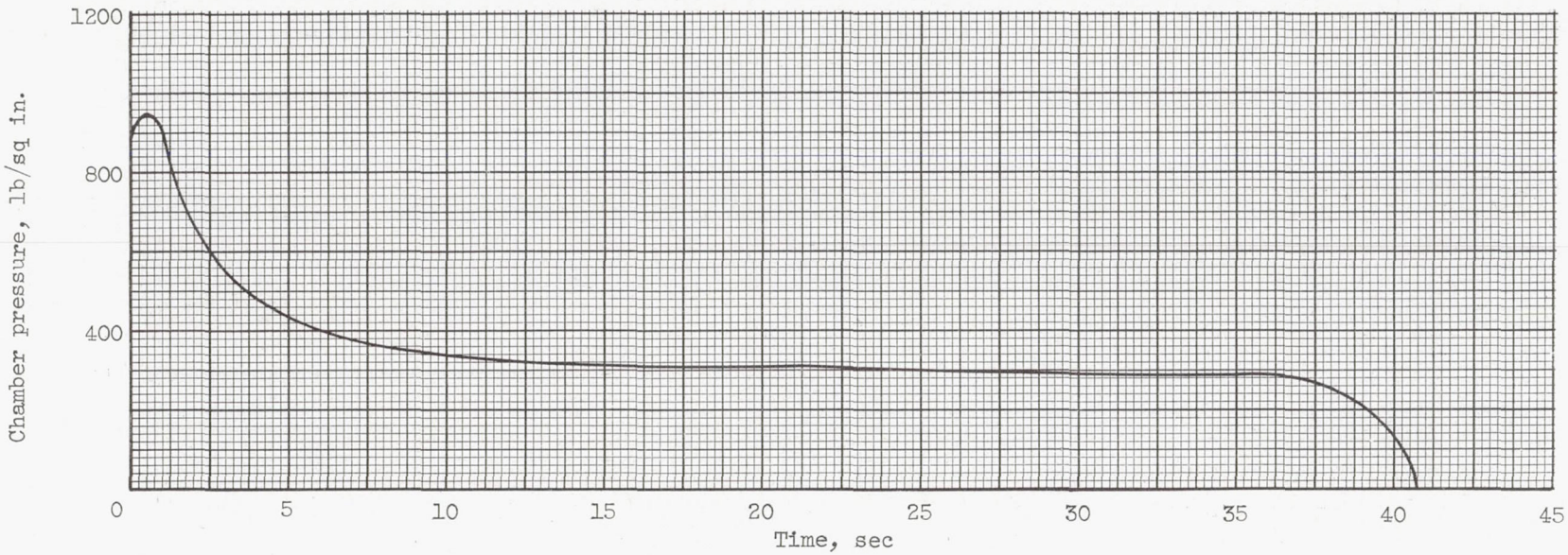

(k) Phenolic-graphite nozzle.

Figure 6. - Continued. Chamber-pressure - time traces obtained during material-evaluation firings.

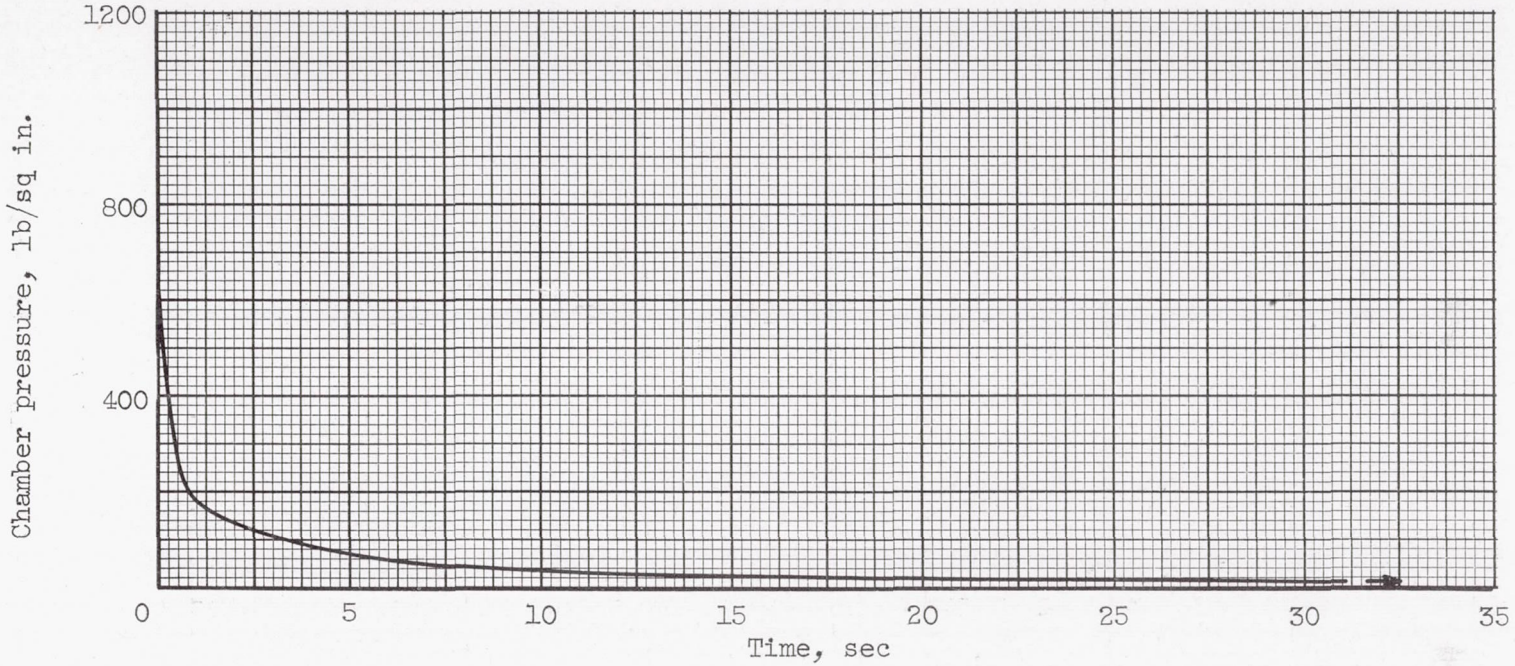

(l) Phenolic-nylon nozzle.

Figure 6. - Concluded. Chamber-pressure - time traces obtained during material-evaluation firings.

(a) Molybdenum nozzle.

Figure 7. - Nozzle-insert-temperature - time traces.

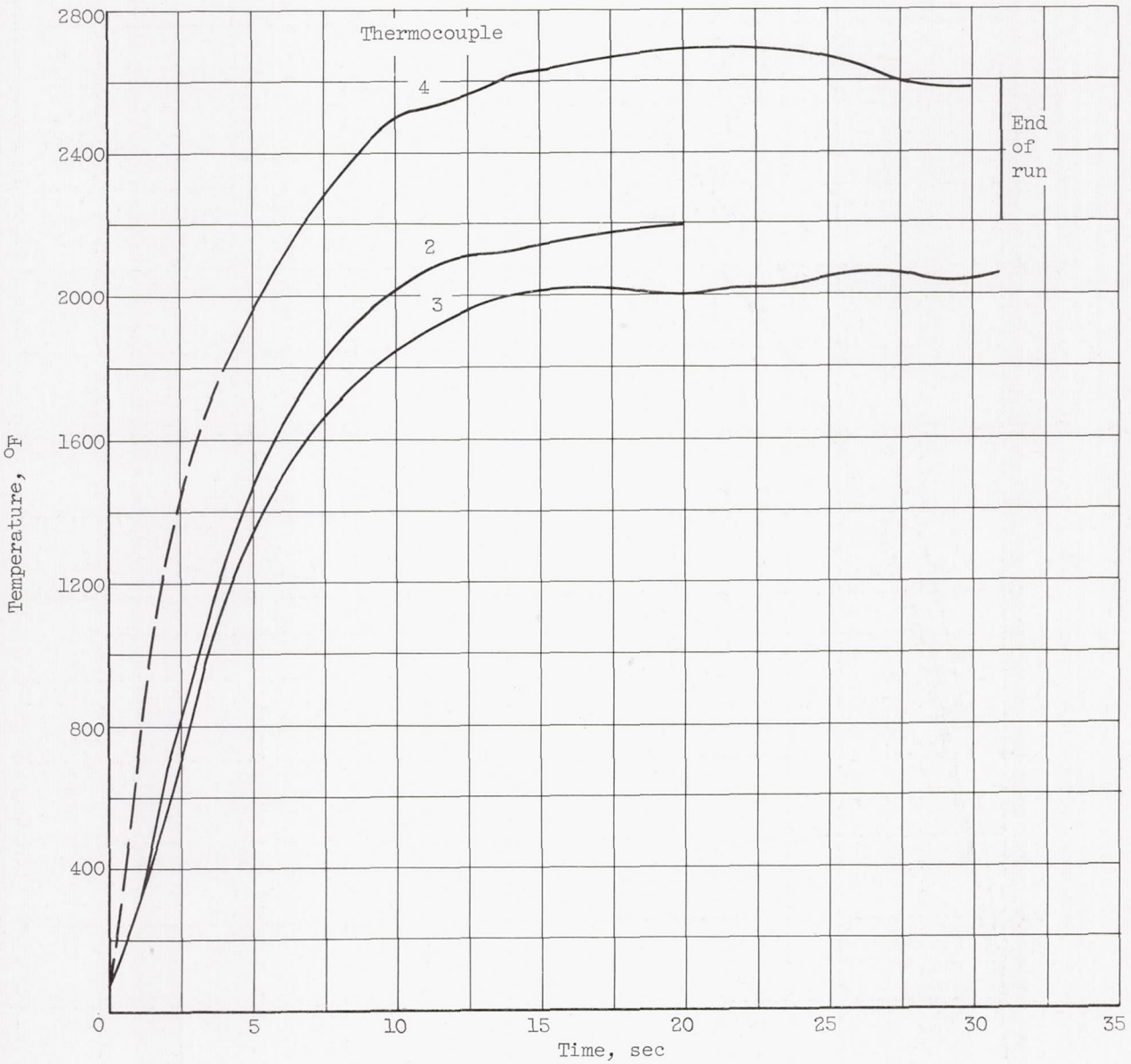

(b) ATJ graphite.

Figure 7. - Continued. Nozzle-insert-temperature - time traces.

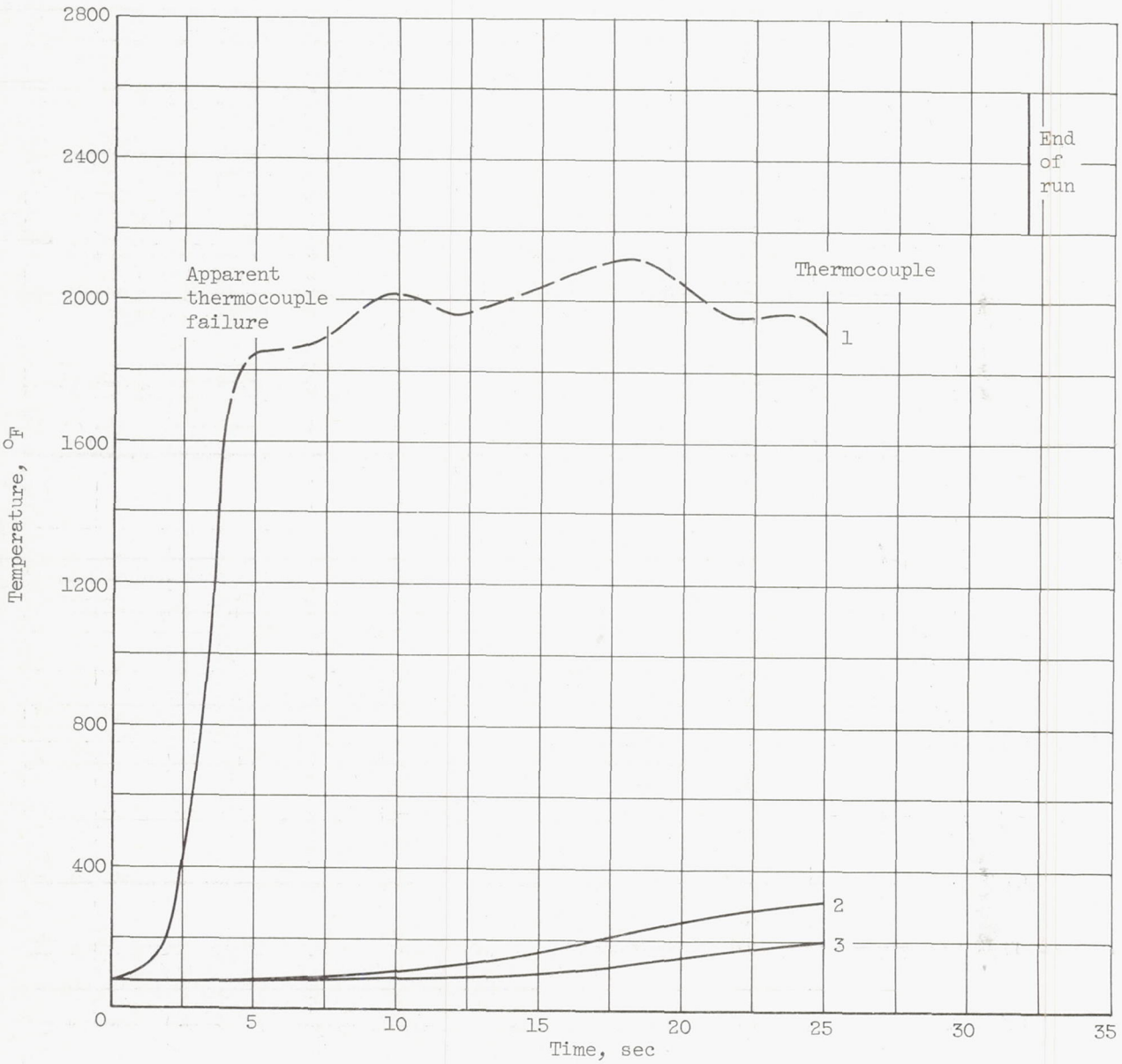

(c) Phenolic-refrasil (40-percent resin) nozzle.

Figure 7. - Concluded. Nozzle-insert-temperature - time traces.

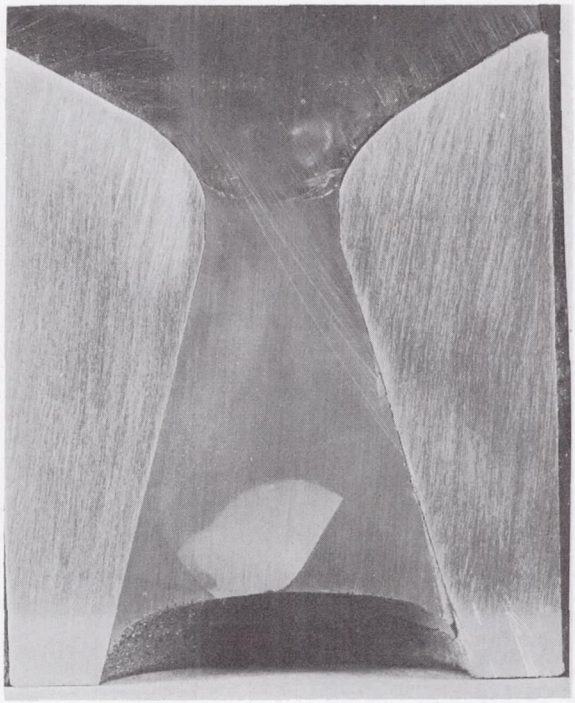

Arc-cast molybdenum

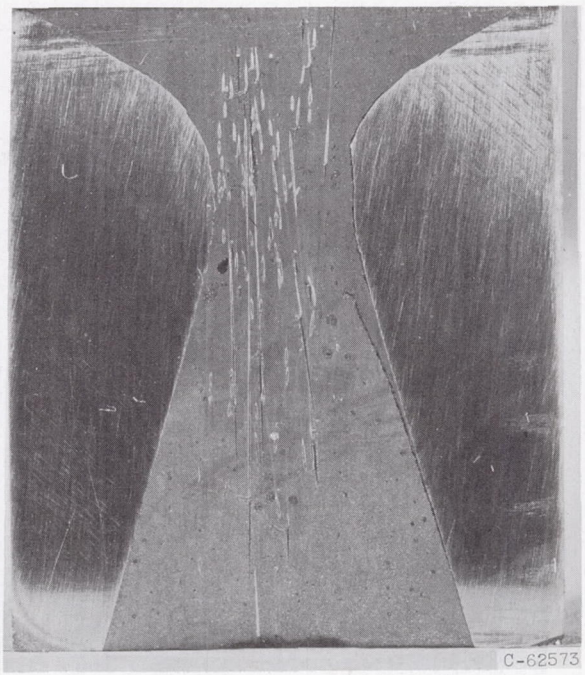

Arc-cast tungsten

(a) Refractory metals.

Figure 8. - Macrophotographs of nozzles after firing.

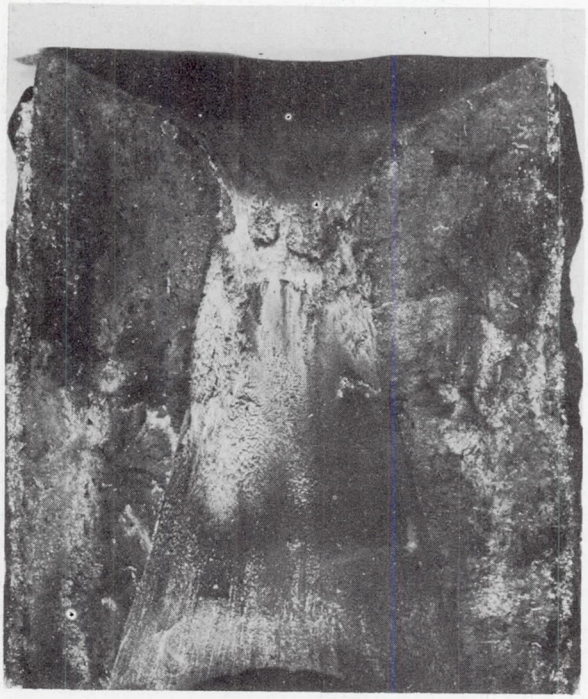

LT1B

LT2

Silicon nitride

(b) Cermets and ceramic.

Figure 8. - Continued. Macrophotographs of nozzles after firing.

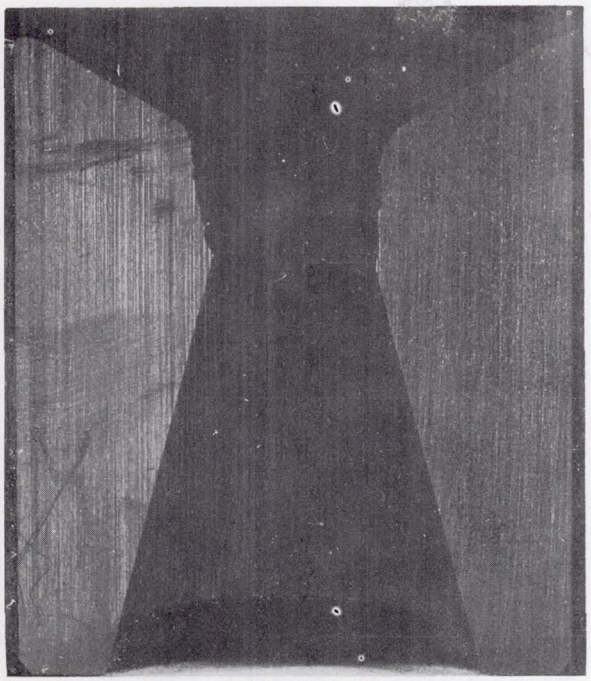

ATJ

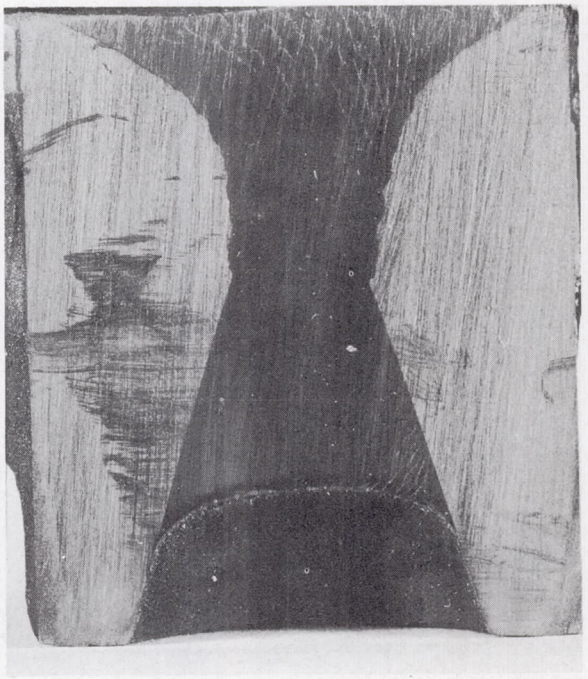

Speer 3499

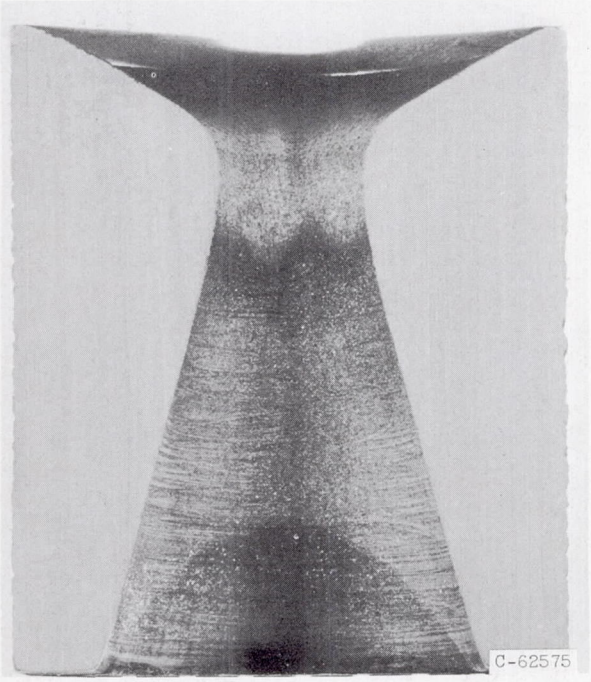

ZT

(c) Graphites.

Figure 8. Continued. Macrophotographs of nozzles after firing.

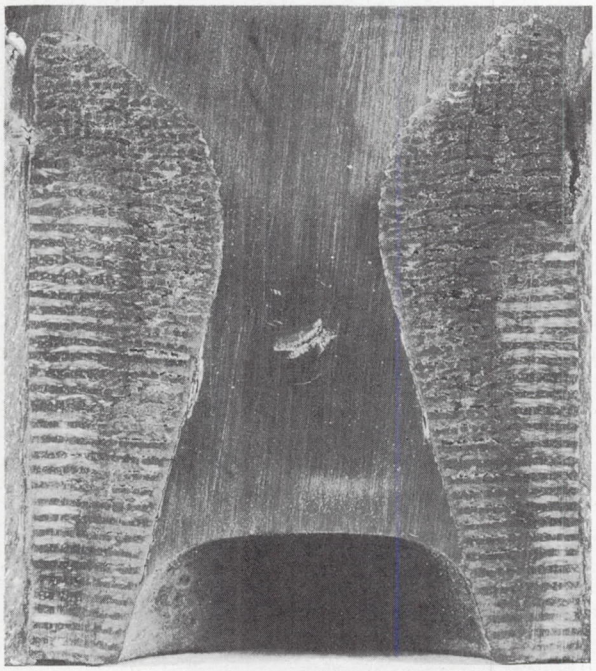

Phenolic refrasil (40-percent resin)

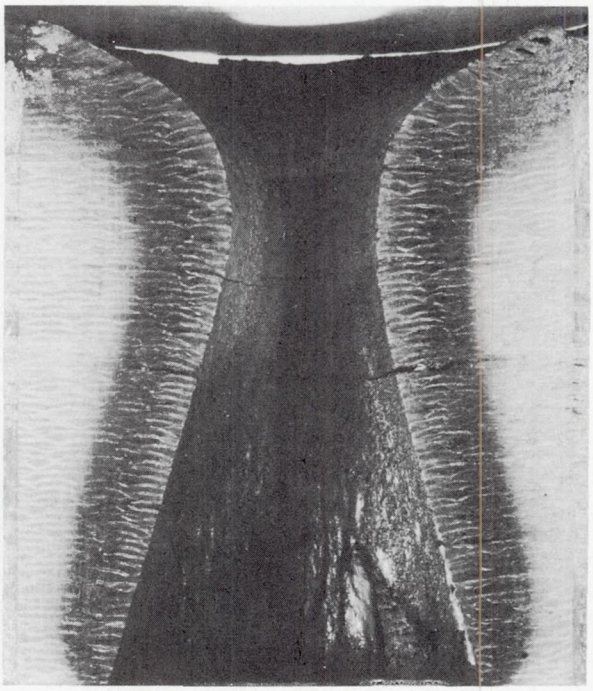

Phenolic refrasil (20-percent resin)

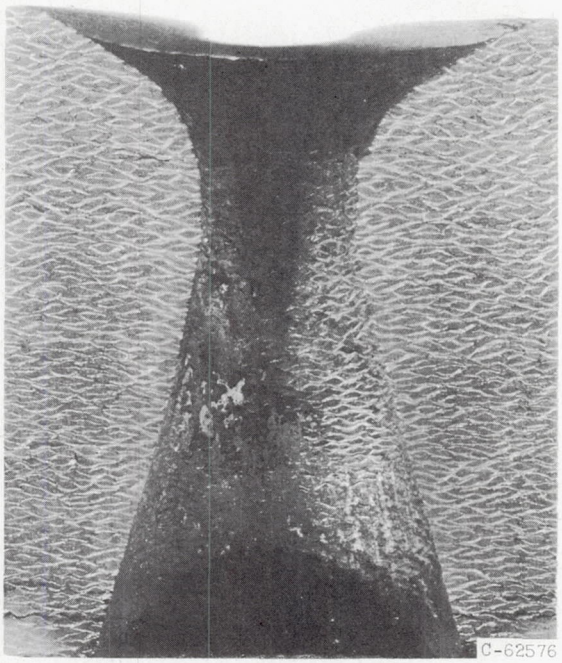

Phenolic graphite

(d) Reinforced plastics.

Figure 8. - Concluded. Macrophotographs of nozzles after firing.

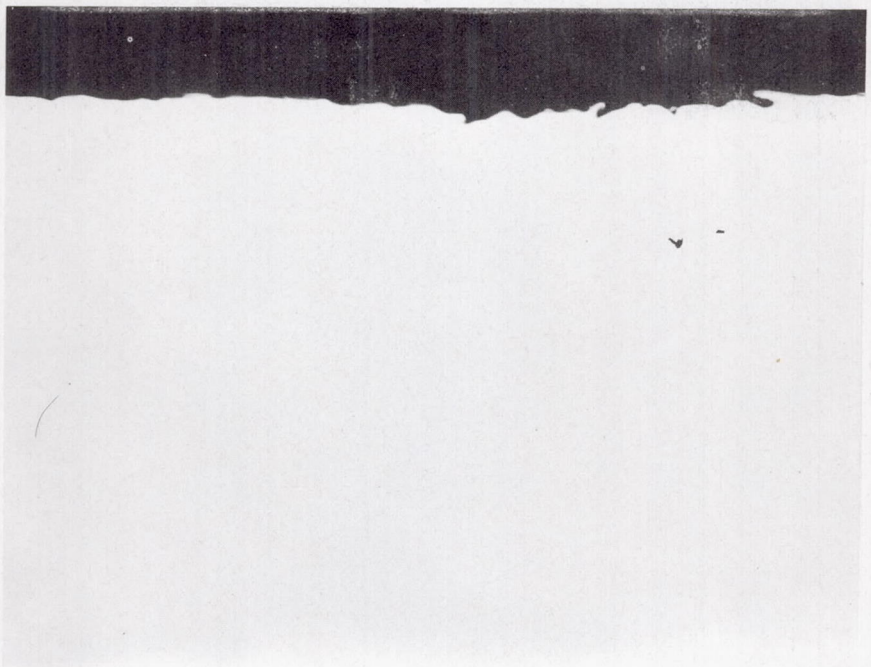

Unetched; ×500

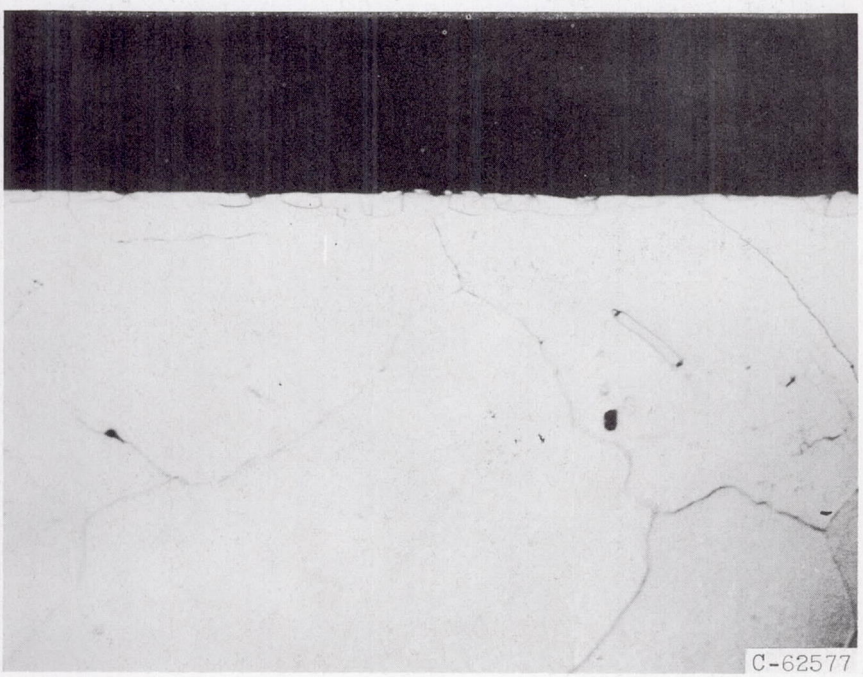

Etchant, potassium ferricyanide; ×500

(a) Molybdenum.

Figure 9. - Photomicrographs of nozzles after firing.

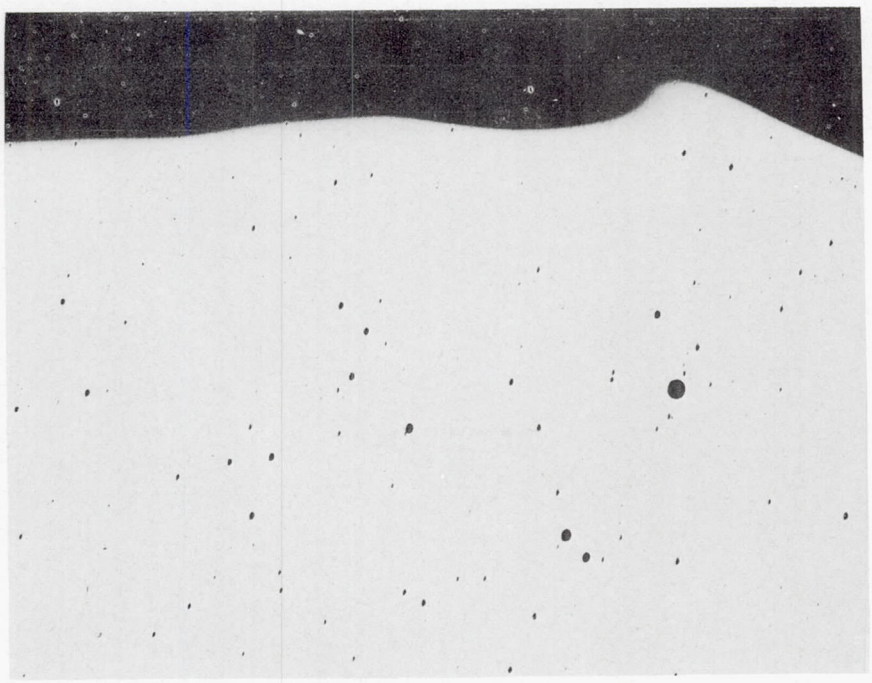

Unetched; ×100

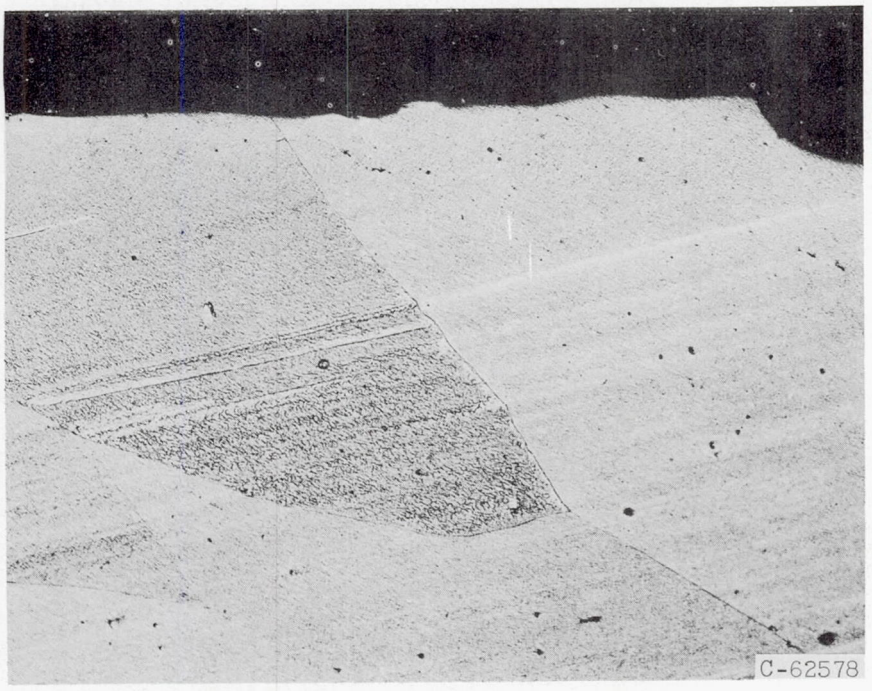

Etchant, potassium ferricyanide; ×100

(b) Tungsten.

Figure 9. - Continued. Photomicrographs of nozzles after firing.

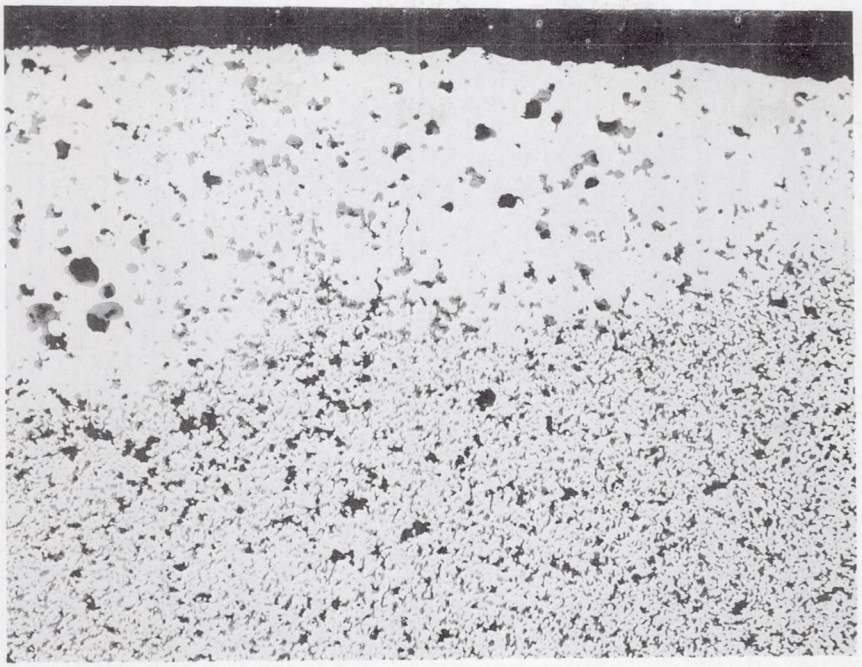

Unetched; ×100

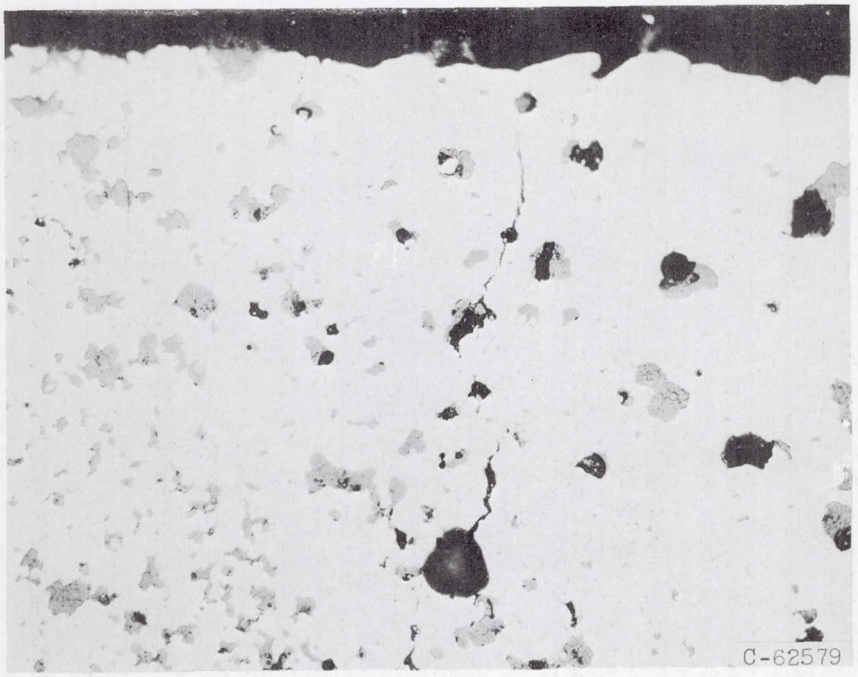

Unetched; ×250

(c) LT2.

Figure 9. - Continued. Photomicrographs of nozzles after firing.

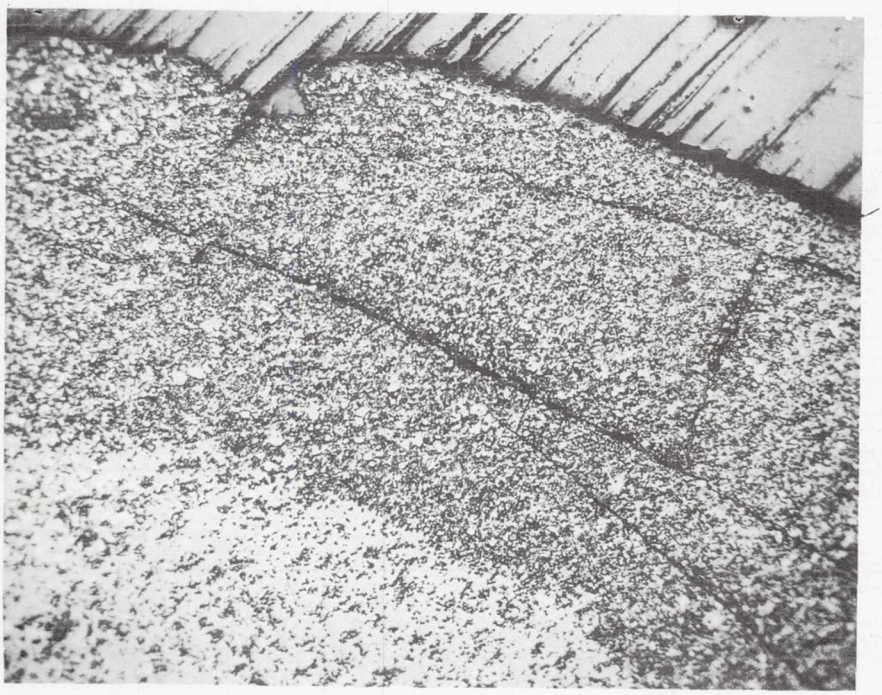

Unetched; ×50

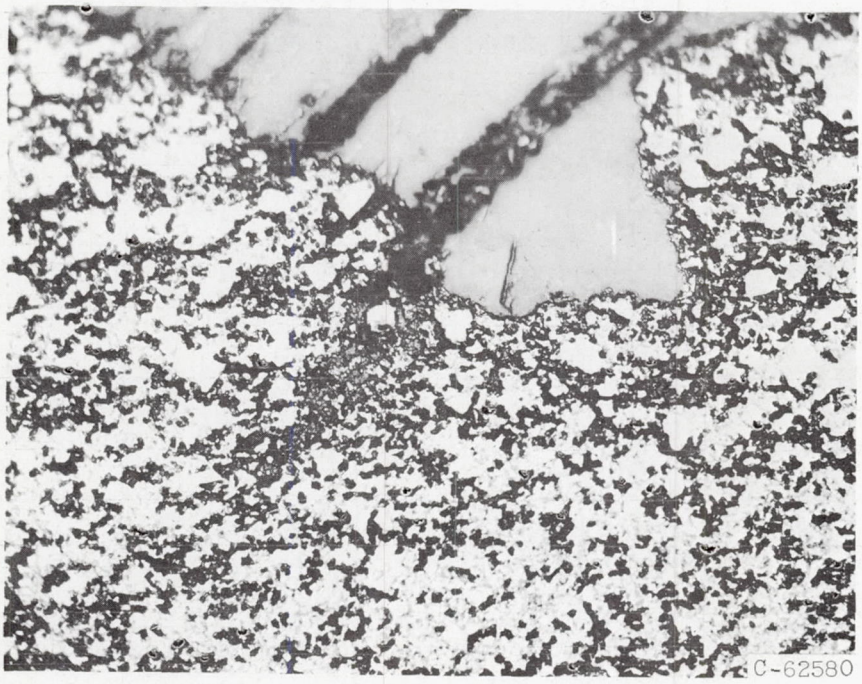

Unetched; ×250

(d) Silicon nitride.

Figure 9. - Concluded. Photomicrographs of nozzles after firing.

NASA-Langley, 1963 E-1815